minerals

MDPI

Article

Trace Element and U–Pb Core Age for Zircons from Western Meiganga Gold Placer, Cameroon: Their Genesis and Archean-Proterozoic Sources

Nguo Sylvestre Kanouo [1,*], Gabriel Ngueutchoua [2], Arnaud Patrice Kouske [3], Rose Fouateu Yongue [2] and Akella Satya Venkatesh [4]

1 Department of Mining Engineering and Mineral Processing, Faculty of Mines and Petroleum Industries, University of Maroua, Maroua 46, Cameroon
2 Department of Earth Sciences, University of Yaoundé I, Yaoundé 812, Cameroon; ngueutchoua2@yahoo.fr (G.N.); rfyongue@yahoo.fr (R.F.Y.)
3 Department of Civil Engineering, The University Institute of Technology, University of Douala, 8698 Douala, Cameroon; arnaudpatricek@gmail.com
4 Department of Applied Geology, Indian Institute of Technology (Indian School of Mines), Dhanbad 826004, India; akellasatyavenkatesh@gmail.com
* Correspondence: sylvestrekanouo@yahoo.fr; Tel.: +237-67896624

Received: 4 March 2018; Accepted: 25 April 2018; Published: 4 May 2018

Abstract: Trace element concentrations and U–Pb ages were obtained using Laser Ablation Split Stream Method from the core of 115 zircon grains from the western Meiganga gold placer deposit. The data was used to characterize zircon, to understand the history of crystallization and to locate source rocks within the local and regional geological settings. Zircon trace element geochemistry was used to distinguish between magmatic and metamorphic affinity. The magmatic zircons have characteristics compatible with their probable origin from granitoid, syenite, tonalite, charnockite and mafic to ultramafic rocks. The metamorphic zircons composition is compatible with growth from anatectic melts and by sub-solidus crystallization in equilibrium with garnet. The zircon ages reveal Archean, Paleoproterozoic, Mesoproterozic, and Neoproterozoic events with the principal source could mainly belong to Paleoproterozoic magmatic lineage. Some of the Paleoproterozoic magmatic zircons were probably sourced from two mica granite found within the local geology, whereas the remaining zircons have features indicating source rocks within the Congo Craton. We suggest that the geologic history of these zircons is related to crustal-scale magmatic and/or tectono-metamorphic events, possibly linked to Eburnean and Pan-African orogeny.

Keywords: Western Meiganga; gold placer; detrital zircon; geochronology; Archean

1. Introduction

Placers are mechanical concentrations of economically viable dense/heavy minerals (e.g., corundum, ilmenite, cassiterite, diamond, rutile, monazite, xenotime, and zircon) and important elements (e.g., gold and platinum, as well as Nb, Ta, and U [1]) sorted and sourced from various areas of erosion within the local and the regional geological settings [2,3]. They are mainly allochthonous in nature, transported and deposited proximally to distally from their source rock [1]. The presence of specific dense and heavy minerals (e.g., zircon, rutile, tourmaline, kyanite, sillimanite, andalusite, and monazite) in placers can be used to track the geological history of the bedrock in the source region [4–15]. Zircon in particular plays a prominent role in provenance studies of displaced and accumulated clastic materials [16–18]. Detrital zircon can be used to make inferences about the source history, for paleogeographic and tectonic reconstitution [19–24]. The use of trace-element geochemistry and U–Pb dating to characterize and interpret the provenance of detrital zircons is well established for constraining source parameters, a commonly used technique in sedimentological and tectonic studies [17,18,25,26]. Hence, geochemical study of detrital or xenocrystic zircon in conjunction with U–Pb geochronology on the same grain is an extremely powerful tracer tool for provenance studies [27].

Gold, zircon and other heavy minerals are found in many areas in Cameroon (e.g., Betaré-Oya in the east; Minton in the south; and Meiganga in the Adamawa). In the Meiganga Sub-division (Figure 1), gold occurs in the south, east, and west. These gold occurrences are mainly found in alluvium and soils, but rarely in primary rocks. In the west of Meiganga Sub-division, gold grains are scattered in sediments from some streams and rivers. There are no known primary gold occurrences in this area, so their source areas have still not been found. In this paper, we used single grain zircon trace element geochemistry and U–Pb core dating to assess the most likely source of the detrital materials associated with gold that is found in substantial quantities in small streams in the west of Meiganga sub-division.

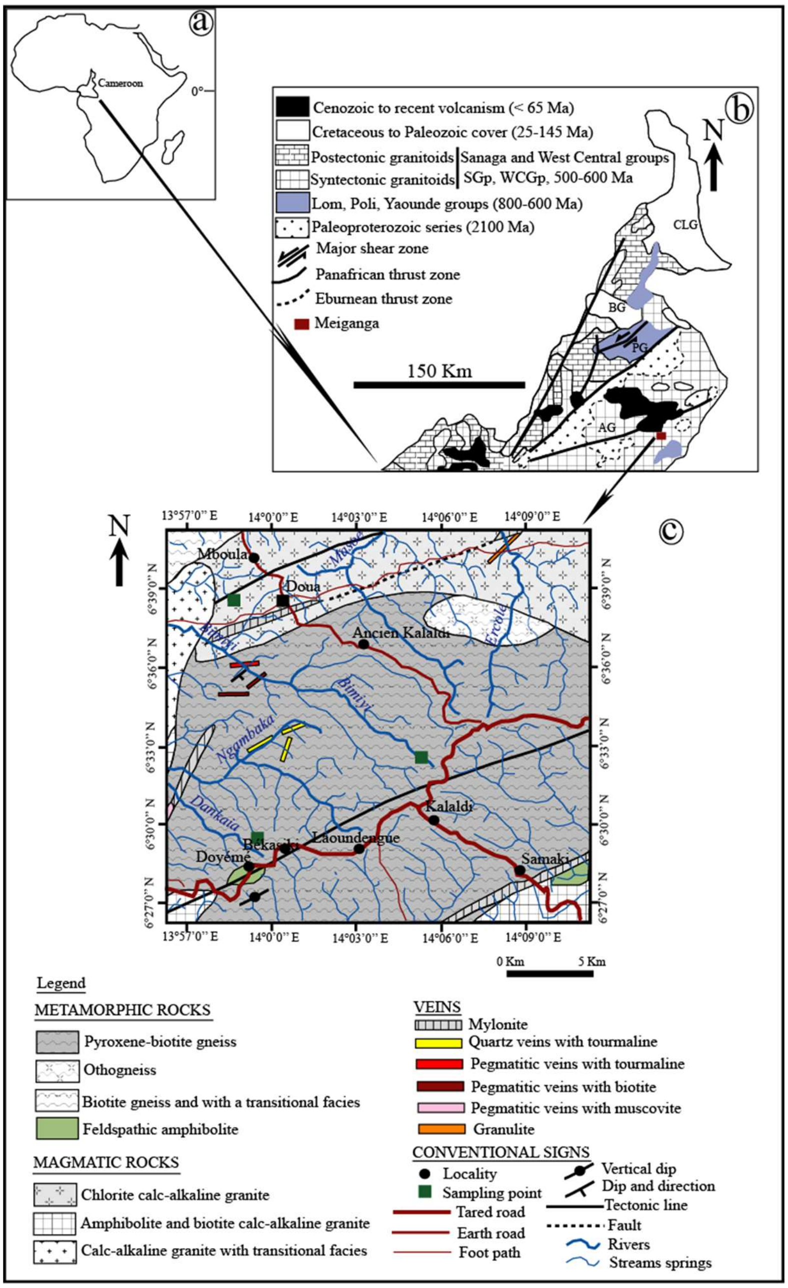

Figure 1. Sketch geologic map locating West of Meiganga within the local and regional settings.

2. Geological Settings

Meiganga is located in the central part of the Pan-African fold belt [28], which is a megatectonic structure formed during the Neoproterozoic and is the product of collision between the Saharan metacraton and the Congo craton [29,30]. This mega-structure covers the main part of the Cameroonian territory and is dominantly composed of pre-Pan-African to syn-Pan-African metamorphic (e.g., gneisses, schists and amphibolites) and igneous rocks (e.g., granite, granodiorite, monzodiorite and monzogranite) [31–39].

Geological formations in Meiganga include: paragneiss, orthogneiss, amphibolite, granulite, migmatite, quartzite, metadiorite, schist, hornfel, and granite [28,35–38,40] which are locally overlain by basalts, sandstones and conglomerates [40]. These rocks are locally covered by red colored soils, eluvium, recent alluvium, and colluvium [41]. Some rocks were intruded by quartzo-feldspathic and syenitic veins (dykelets), doleritic and micrograntic dykes probably formed within the fracture network of the host rocks [28,40]. Shear zones and mylonites [40] are found in some of the metamorphic basement rocks and were interpreted to represent the products of syn-tectonic ductile and cataclastic deformation [28]. Some of the gneisses and amphibolites underwent retrograde metamorphism that led to the formation of greenschist facies mineral assemblages [28,38]. Partial melting of gneiss led to the crystallization of leucogranites found in the northern part of Meiganga [37]. The inherited magmatic zircon ages (2339–1887 Ma and 889–675 Ma) for amphibole-biotite gneiss (locally found) indicate that part of the zircons in this rock were sorted from igneous protoliths [36]. Metadioritic basement rock (with age ranging from 619–614 Ma) was formed during syn-tectonic events [28,37].

The western part of Meiganga, from where the studied detrital zircons were sampled, is locally made up of pyroxene-amphibole banded gneiss, and both calc-alkaline and two mica granites [28,40]. Pyroxene-amphibole banded gneiss (with zircon ages ranging from 2602–2504 Ma, 2478–1685 Ma, and 901 to 550 Ma) outcrops mainly in two villages (Kalaldi and Doua) [28,38]. This rock partly encloses syenitic veins striking parallel in the NW-SE direction [28] and amphibolites [40].

3. Materials and Methods

In total, one hundred and fifteen zircon grains were analyzed for their trace element contents and U–Pb ages at the University of California, Santa Barbara, CA, USA. The analyzed zircons were sampled from small, nameless, first order tributary streams found in the study area (Figure 1c), similar to the sampling strategy employed in [42]. According to [42], during gold exploration, it is better to sample small streams (first-order tributaries) where the streams are <5 km in length rather than larger rivers, because the former yield more valuable information on the provenance of placer gold than samples from large rivers. Collected samples (5 kg $\times$ 10) in each point (from gravel layer) and from three localities (Békasiki, Doua, and Kaladi: see Figure 1c) were washed (by panning) immediately in the field and on the spot to obtain substantial quantity of heavy mineral concentrates. Each concentrate was packaged separately, numbered and carried to the laboratory for gold identification and heavy mineral separation. Heavy mineral concentrates with gold grains were separated using dense liquid (bromoform: $D \geq 2.7$ g/cm^{-3}) at the Department of Earth Sciences at the University of Yaoundé I, Cameroon. The mineral separation protocols are similar to those described in [43] and [44]. A pre-concentrated gold-host heavy mineral assembly (from Békasiki) was sent to the University of California (Santa Barbara, CA, USA) for the zircon grains separation and analyses by Laser Ablation Split Stream.

Zircon U/Pb geochronology and trace element data were acquired simultaneously using a laser ablation "split stream" setup consisting of a Photon Machines Excimer 193 nm laser ablation unit coupled to a Nu Instruments, "Nu Plasma" multi-collector inductively coupled plasma-mass spectrometer and an Agilent 7700S quadrupole inductively coupled plasma-mass spectrometer, housed at the University of Santa Barbara, CA, USA (for detailed methodology see [45–47]). Samples were analyzed for 20 s using a fluence of 1.5 J/cm^2, a frequency of 4 Hz, and spot size of 20 µm diameter resulting in crater depths of ~9 µm. Utilizing a standard-sample bracketing technique, analyses of reference materials with known isotopic compositions were measured before and after each set of seven unknown analyses. Data reduction, including corrections for baseline, instrumental drift, mass bias, down-hole fractionation, and age and trace element concentration calculations were carried out using Iolite v. 2.1.2 [48]. "91,500" zircon (1065.4 ± 0.3 Ma $^{207}Pb/^{206}Pb$ ID-TIMS age and 1062.4 ± 0.4 Ma$^{206}Pb/^{238}U$ ID-TIMS age: [49]) served as the primary reference material to monitor and correct for mass bias, as well as Pb/U down-hole fractionation and to calibrate concentration data, while "GJ-1" zircon (608.5 ± 0.4 Ma $^{207}Pb/^{206}Pb$ and 601.7 ± 1.3 Ma $^{206}Pb/^{238}U$ ID-TIMS ages: [50]) was treated as an unknown in order to assess accuracy and precision. Twenty-three analyses of GJ-1 zircon throughout the analytical session yield a weighted mean $^{207}Pb/^{206}Pb$ date of 593 ± 5 Ma, MSWD = 0.8 and a weighted mean $^{206}Pb/^{238}U$ date of 603 ± 2 Ma, MSWD = 1.0. Concordia and Kernal Density Estimate (KDE) plots were calculated in Isoplot v 2.4 [51] and Density Plotter [52], respectively, using the ^{238}U, and ^{235}U decay constants of [53]. All uncertainties are quoted at 95% confidence levels or 2 s level and include contributions from the external reproducibility of the primary reference material for the $^{207}Pb/^{206}Pb$ and $^{206}Pb/^{238}U$ ratios. For plotting and age interpretation purposes, the $^{207}Pb/^{206}Pb$ dates are used for analyses older than 1000 Ma, whereas the $^{206}Pb/^{238}U$ dates are used for analyses younger than 1000 Ma.

4. Results

4.1. Zircon Geochemistry

Twenty three elements (Table 1) quantified from the zircon cores are heterogeneous, as is expected with their elemental concentration ranges similar to those reported in the literature. Within these elementary suites, Hf and Y are minor, whereas other 21 elements (U, Th, Pb, Ti, Nb, Ta, Sr, and REE) are mainly at trace levels. The minor and trace elements concentrations are presented separately.

Table 1. Minor and trace elementary abundance (in ppm) in the western Meiganga detrital zircons.

Spot/Grain Number	Hf	Y	U	Th	Pb	Ti	Nb	Ta	Sr	Hf/Y	Th/U	Nb/Ta	Ti-in-Zircon T	
													°C	±2σ
MW001	12,580	720	451	14	4	2.4	2.1	3.04	0.19	17.47	0.032	0.691	62	106
MW002	10,410	228	83	40	47	15.1	0.5	0.56	0.06	45.66	0.477	0.891	786	154
MW003	10,950	387	55	137	128	8.3	1.5	1.49	0.1	28.3	2.457	1.007	729	58
MW004	11,300	1065	220	307	289	9.4	4.4	3.79	0.19	10.61	1.383	1.161	740	48
MW005	12,380	571	169	153	143	10	2.2	2.19	0.14	21.68	0.91	1.005	746	74
MW006	12,140	1014	799	285	140	58.8	4	7.84	0.49	11.97	0.355	0.511	945	42
MW007	12,850	412	126	55	56	9	1.4	1.95	0.07	31.19	0.431	0.718	736	109
MW008	10,800	595	249	170	189	8.2	1.2	0.93	0.12	18.15	0.683	1.291	728	61
MW009	12,710	702	302	271	243	15.1	4.1	3.23	0.15	18.11	0.894	1.269	786	68
MW010	11,900	1109	288	409	341	7.7	2.4	2.02	0.14	10.73	1.418	1.188	722	40
MW011	11,690	1186	222	393	360	5.6	4	2.58	0.27	9.86	1.776	1.551	694	73
MW012	10,780	621	107	165	222	8.7	2.8	1.37	0.1	17.36	1.531	2.044	733	66
MW013	10,550	354	84	38	42	4.1	0.4	0.31	0.13	29.8	0.429	1.291	669	81
MW014	11,510	1104	326	447	401	5.1	2.7	2.15	0.16	10.43	1.37	1.256	686	71
MW015	12,380	136	212	8	8	3.8	1	2.15	0.05	91.03	0.038	0.465	662	58
MW016	12,020	204	223	60	73	5.8	0.9	1.32	0.06	58.92	0.267	0.682	697	57
MW017	11,710	910	210	260	251	6.2	2	1.63	0.13	12.87	1.238	1.227	703	67
MW018	12,340	702	259	184	149	12.8	4.8	3.24	0.11	17.58	0.707	1.482	770	35
MW019	12,170	435	236	208	233	6.9	1	1.78	0.13	27.98	0.881	0.562	712	47
MW020	6390	144	100	46	58	7	0.8	0.83	0.04	44.38	0.461	0.964	713	35
MW021	11,030	460	257	309	282	8.3	2.3	2.15	0.11	23.98	1.202	1.07	729	53
MW022	10,960	622	204	13	4	3.9	2.5	2.2	0.17	17.62	0.065	1.136	665	89
MW023	13,020	824	1042	432	168	47	2.2	3.48	1.79	15.8	0.409	0.632	915	41
MW024	11,210	1747	713	859	443	19.9	5.6	3.52	3.1	6.42	1.215	1.591	815	25

Table 1. *Cont.*

Spot/Grain Number	Hf	Y	U	Th	Pb	Ti	Nb	Ta	Sr	Hf/Y	Th/U	Nb/Ta	Ti-in-Zircon T	
													°C	±2σ
MW025	12,150	535	107	58	58	4.9	1.3	1.12	0.12	22.71	0.539	1.161	683	58
MW026	10,640	465	67	63	77	13.9	0.9	0.7	0.09	22.88	0.947	1.286	778	73
MW027	10,920	470	316	255	224	7.3	4.2	3.24	0.08	23.24	0.791	1.296	717	59
MW028	11,020	524	211	173	166	3.9	2.5	2.1	0.13	21.03	0.824	1.191	665	75
MW029	10,690	730	224	248	246	6.1	3.5	2.65	0.12	14.64	1.105	1.321	701	65
MW030	10,960	790	210	314	314	15.2	3.6	3.07	0.16	13.87	1.477	1.173	787	75
MW031	10,640	562	362	268	216	7.7	4.6	2.94	0.13	18.93	0.736	1.565	722	35
MW032	9240	237	117	56	75	6.9	1	0.81	0.04	38.99	0.477	1.235	712	44
MW033	10,860	405	292	247	213	6	4.6	3.09	0.09	26.82	0.842	1.489	700	69
MW034	10,250	141	437	93	100	3.3	0.6	1.28	0.04	72.7	0.21	0.469	651	59
MW035	10,990	1230	220	309	301	5.6	2.5	2.19	0.27	8.94	1.402	1.142	694	63
MW036	10,760	1477	304	616	618	3.8	3.1	2.34	0.25	7.29	2.012	1.325	662	58
MW037	10,610	901	148	300	292	5.7	2.4	2.08	0.17	11.78	2.024	1.154	696	86
MW038	10,470	808	250	372	364	5.7	4.4	3.57	0.17	12.96	1.468	1.233	696	79
MW039	8370	90	218	60	73	7.1	0.2	0.09	0.05	93	0.274	2.222	715	40
MW040	10,320	747	197	297	290	5.2	3.5	3.14	0.23	13.82	1.49	1.115	688	74
MW041	9850	613	87	132	176	5.6	1.6	1.71	0.13	16.07	1.522	0.936	694	66
MW042	9950	710	218	307	287	5.8	3.5	2.78	0.14	14.02	1.393	1.259	697	44
MW043	11,310	953	344	413	400	5.3	3.1	2.14	0.18	11.87	1.203	1.449	690	69
MW044	11,270	830	293	83	78	4.3	2.1	2.42	0.18	13.58	0.285	0.868	672	52
MW045	9450	598	166	194	189	6	2.5	1.93	0.12	15.81	1.175	1.295	700	46
MW046	9910	1466	299	624	607	4.9	2.3	2.64	0.23	6.76	2.096	0.871	683	47
MW047	8840	352	79	122	123	4.6	2.1	2.15	0.07	25.12	1.563	0.977	678	66
MW048	12,500	166	189	47	45	133	0.8	0.75	0.09	75.3	0.249	1.067	1065	79
MW049	10,080	782	93	262	259	6	3.5	2.54	0.15	12.89	2.822	1.378	700	62
MW050	11,120	412	196	126	154	5.3	1	1.39	0.13	26.99	0.643	0.719	690	58
MW051	9700	354	135	99	108	7.4	1.7	2.32	0.17	27.4	0.743	0.733	718	127
MW052	9050	82	115	4	1	1.3	0.6	0.99	0.05	110.37	0.038	0.606	584	88
MW053	10,100	482	280	225	186	6	2.4	1.83	0.07	20.96	0.81	1.312	700	56
MW054	10,950	491	343	289	349	7.3	1.2	1.8	0.14	22.3	0.842	0.667	717	53
MW055	9060	545	392	132	171	8.7	1.3	1.39	0.17	16.63	0.328	0.935	733	63
MW056	10,420	447	988	316	152	32.5	3.2	4.81	3.48	23.31	0.321	0.665	870	28
MW057	10,060	313	112	90	90	8.2	1.2	1	0.13	32.14	0.796	1.2	728	66
MW058	10,900	413	230	6	2	1.4	2.8	4.77	0.2	26.39	0.025	0.587	589	61
MW059	10,470	460	233	161	149	3.9	2.4	2.64	0.12	22.76	0.684	0.909	665	66
MW060	10,240	393	202	154	151	5.8	3	2.61	0.09	26.06	0.762	1.15	697	41
MW061	9970	505	120	86	107	2.8	1.5	1.59	0.16	19.74	0.716	0.943	638	42
MW062	9760	916	231	328	333	4.1	2.3	2.09	0.2	10.66	1.379	1.101	669	59
MW063	9620	472	370	282	261	6.2	4.3	2.91	0.13	20.38	0.759	1.478	703	54
MW064	10,170	795	389	174	163	4.6	4.3	3.33	0.17	12.79	0.446	1.291	678	49
MW065	11,810	244	127	2	1	2.2	1.5	2.63	0.09	48.4	0.014	0.57	621	70
MW066	9700	441	297	273	263	4.5	3.9	2.58	0.11	22	0.93	1.512	676	50
MW067	10,410	337	422	60	65	9.8	0.7	1.28	0.23	30.89	0.139	0.547	744	66
MW068	9580	392	126	169	170	4.5	2	1.49	0.07	24.44	1.342	1.342	676	63
MW069	9720	478	249	218	213	4.5	3.9	2.67	0.12	20.34	0.887	1.461	676	63
MW070	9080	313	101	111	112	3.1	2.1	1.7	0.09	29.01	1.109	1.235	646	39
MW071	9920	616	385	106	117	3.8	1.4	1.99	0.18	16.11	0.278	0.704	662	58
MW072	9400	348	267	77	94	2	0.9	1.2	0.06	27.01	0.288	0.75	613	55
MW073	9850	345	165	194	179	4.6	3	2.09	0.1	28.55	1.178	1.435	678	45
MW074	9700	567	301	211	197	3.8	1.5	1.67	0.18	17.11	0.708	0.898	661	47
MW075	9670	554	243	307	278	5.6	3.5	2.94	0.13	17.46	1.269	1.191	694	45
MW076	8660	210	480	101	141	5.2	0.7	1.19	0.06	41.24	0.209	0.588	688	34
MW077	8940	755	258	392	400	4.1	4.9	3.24	0.15	11.84	1.527	1.513	669	33
MW078	9410	360	171	143	139	4.4	2.5	2.45	0.11	26.14	0.828	1.021	674	51
MW079	9770	458	269	209	206	3.9	3.8	2.89	0.1	21.33	0.778	1.315	664	40
MW080	8910	292	494	97	138	2.7	0.7	1.19	0.05	30.52	0.195	0.588	636	77
MW081	9430	81	255	50	55	2.1	0.3	0.84	0.05	116.42	0.194	0.357	618	87
MW082	9630	626	358	160	158	4.4	2.9	3.53	0.14	15.38	0.449	0.822	674	68
MW083	9530	335	407	17	5	1.3	1.4	2.39	0.08	28.45	0.042	0.586	584	99

Table 1. *Cont.*

Spot/Grain Number	Hf	Y	U	Th	Pb	Ti	Nb	Ta	Sr	Hf/Y	Th/U	Nb/Ta	Ti-in-Zircon T	
													°C	±2σ
MW084	9240	134	280	70	74	2.6	0.5	0.95	0.06	68.96	0.25	0.526	633	66
MW085	8030	218	67	144	146	3.2	1.2	0.89	0.07	36.84	2.132	1.348	649	55
MW086	9490	665	204	198	193	38.9	4.3	2.42	0.19	14.27	0.968	1.777	892	62
MW087	9010	467	115	121	123	3.8	2.5	2.39	0.1	19.29	1.065	1.046	662	53
MW088	9350	700	170	221	227	3.4	2	1.42	0.17	13.36	1.307	1.408	654	63
MW089	8760	590	229	200	185	3.8	3.9	2.67	0.32	14.85	0.862	1.461	661	39
MW090	7020	327	86	90	134	3.6	1.9	0.98	0.07	21.47	1.057	1.939	658	60
MW091	9240	1494	273	435	437	4.1	2.7	2.05	0.24	6.18	1.582	1.317	669	63
MW092	9160	615	210	269	248	3.1	3.4	2.89	0.14	14.89	1.267	1.176	647	63
MW093	9160	1867	353	462	629	5.3	4.8	3.24	0.42	4.91	1.323	1.482	690	66
MW094	9190	898	249	207	197	4.3	2.9	2.77	0.16	10.23	0.831	1.047	672	51
MW095	9310	554	281	494	466	5.1	4.5	2.6	0.12	16.81	1.748	1.731	686	45
MW096	9780	1134	649	651	713	14.3	6.9	4.27	0.27	8.63	1.012	1.616	781	152
MW097	7570	750	71	145	180	7.6	0.8	1.33	0.16	10.09	2.024	0.602	721	89
MW098	9540	217	374	81	104	2.3	0.6	1.18	0.03	43.96	0.214	0.508	623	66
MW099	10,000	781	345	280	287	4.3	2.9	2.69	0.17	12.81	0.816	1.078	672	48
MW100	7500	119	11	21	34	7.4	0.3	0.27	0.04	63.03	1.957	1.111	718	155
MW101	9300	210	231	107	128	5.4	0.9	0.96	0.16	44.29	0.456	0.938	691	57
MW102	10,360	283	177	58	55	4.3	1.7	1.78	0.06	36.61	0.322	0.955	672	65
MW103	9790	333	70	113	115	4.7	1.4	1.5	0.07	29.4	1.613	0.933	679	34
MW104	9820	159	380	94	104	4.7	0.8	0.95	0.1	61.76	0.246	0.842	680	56
MW105	8970	533	233	275	267	5.8	3.8	3.3	0.13	16.83	1.174	1.152	697	44
MW106	9320	349	197	156	144	5.5	1.4	1.45	0.11	26.71	0.784	0.966	693	67
MW107	9470	275	318	68	87	1.9	0.6	1.31	0.08	34.44	0.213	0.458	612	82
MW108	11,460	421	115	23	30	3.8	1.7	2.28	0.1	27.22	0.195	0.746	662	43
MW109	9550	988	280	320	335	9.2	2.2	2.05	0.22	9.67	1.142	1.073	738	65
MW110	8540	451	145	165	259	7.9	0.7	0.71	0.12	18.94	1.14	0.986	724	53
MW111	9040	471	167	172	182	6.5	1.4	1	0.2	19.19	0.991	1.4	707	71
MW112	9720	261	167	45	52	4.5	0.6	0.27	0.09	37.24	0.268	2.222	676	54
MW113	7120	244	31	10	15	3.9	0.4	0.23	0.06	29.18	0.306	1.739	664	46
MW114	10,070	1502	295	641	659	9.6	3.4	2.47	0.26	6.71	2.193	1.377	742	65
MW115	10,260	448	189	17	5	1.1	2	3.74	0.12	22.91	0.092	0 .535	571	114

4.1.1. Minor Elements

Hafnium varies between 6390 and 13,020 ppm, which is in general higher than values reported for detrital zircons from western Mamfe area [10–12]. Most of the values are above 9000 ppm with very few being below 7500 ppm. Some zircons have similar abundances (e.g., Hf = 9160 ppm in MW092 and MW093), suggesting same degree of Hf substitution (degree of fractionation) in these zircons. Due to the high heterogeneity of the Hf contents, the zircon grains can be classified into three main groups: (1) relatively low-Hf zircons (Hf ≤ 8910 ppm); (2) moderate-Hf zircons (9010 ppm ≤ Hf ≤ 10,120 ppm); and (3) high-Hf grains (Hf > 10,120 ppm). The Hf values in group 1 are within the range in magmatic zircons crystallized in a continental rift setting (Hf < 9000 ppm: cf. [27]) whereas those in the other group could be that of zircons grew out of rifting.

Yttrium content ranges from 82 to 1867 ppm with the lowest value found in NW081, and the highest in MW093. They are generally greater than 250 ppm, with a few values exceeding 1000 ppm. Four groups can be distinguished; (1) zircons with relatively low Y (<160 ppm); (2) zircons with moderately low Y (204–491 ppm); (3) zircons with relatively high Y (505–988 ppm); and (4) zircons with very high Y (≥1014 ppm). The Y values are mostly within the range noted in [54] and [55] for crustal derived zircons, with some being close to values found in [19] high-Si granitoids. The calculated Hf/Y ratios for the zircon grains vary from 4 to 117 with the lowest values found in MW093 and the highest in MW081.

4.1.2. Trace Elements

The U values, listed in Table 1, ranges from 11 to 1042 ppm with the lowest values mainly found in MW100 and MW113 and the highest in MW023 and MW096. Some zircons have similar contents (e.g., U = 210 ppm in MW017 and M030, or U = 222 ppm: MW11 and U = 223 ppm: M016), suggesting same degree of U substitution in those grains [11,12]. Those with very low U (<30 ppm) values are within the range limit in [54] kimberlitic and [55] syenitic zircons. Zircons with U > 300 ppm are close to those in detrital zircons classified as from high-Si granitoids [19], and within the range noted by [56] for granitic zircons.

Thorium content ranges from 2 to 859 ppm, with some values being much higher than others. They can form three groups: (1) made up of zircons with Th ≤ 70 ppm; (2) zircons with Th (70–101 ppm), and (3) composed of grains with Th ≥ 106 ppm. Correlation exists between the Th and U values in Figure 2a, for zircons whose Th and U contents are <520 ppm and <400 ppm, respectively. The calculated Th/U ratios (0.01 to 2.80) are highly heterogeneous. Due to the heterogeneity of the Th/U ratios, the zircons can be grouped into two: (1) those with Th/U ratio (<0.07) compatible with metamorphic zircons [57] and (2) those with magmatic zircons (0.2 ≤ Th/U ≤ 1: [58]). The Th/U versus Th binary diagram (Figure 2b) shows positive correlation, whereas no correlations are evident in the Th/U versus U diagram (Figure 2c).

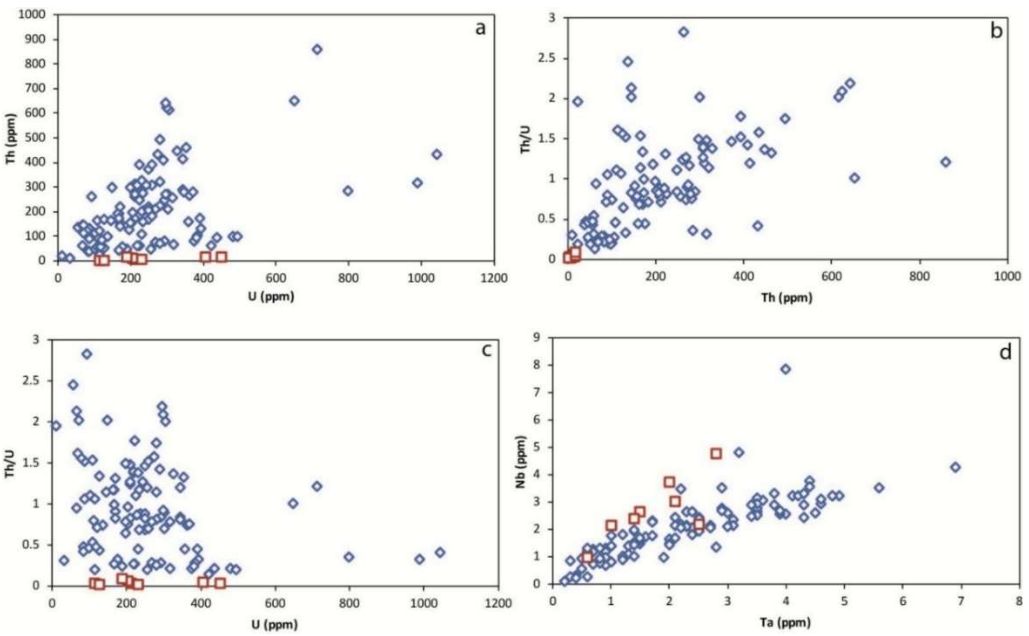

Figure 2. Geochemical correlation of various elements/ratios within the western Meiganga detrital zircons (**a**): Th versus U; (**b**): Th/U versus Th; (**c**): Th/U versus U; (**d**) Nb versus Ta; blue and white diamond-shape plots are for magmatic zircons; red and white square plots are for metamorphic zircon).

The lead content ranges from 1.0 to 713 ppm. The lowest values were obtained in MW052, MW058, and MW065, and the highest in MW095 and MW114. It is noted that some zircons with very low Pb value also have very low Th, with similar Th (Th = 8 ppm: MW015) and Pb (Pb = 8 ppm: MW015) being found in the same grain. Some grains have the same Pb content (e.g., Pb = 149 ppm: MW018 and MW059).

Titanium content ranges from 1.1 to 133 ppm, with most values not exceeding 7.5 ppm. The lowest values are mainly found in NW115 and MW052, and the highest in MW048. Zircons with very low Ti value show very low Pb and Th contents. The calculated Ti-zircon temperatures (estimated Ti activity of 1) range from 571 to 1065 °C (Table 1), with most of the lowest temperatures calculated for zircon with very low Th/U ratio (≤0.09), and the highest temperature (≈1065 °C) calculated for zircon with low Th/U ratio (≈0.25). Some grains have similar temperature or very close values; this may reflect crystallization at the same conditions.

Niobium (0.2–7.0 ppm) and Ta (0.09–8.0 ppm) contents are very low. Most Nb contents are close to that of Ta and show a positive correlation in Figure 2d. The Nb/Ta ratios vary from 0.40 to 2.23 with most of values being slightly greater than 1.

4.1.3. Rare Earth Elements

The quantified rare earth element abundances are highly heterogeneous (Table 2). Within the LREE suite, La is predominantly below detection, except in MW001 and MW115. The Ce content ranges from below detection to 330 ppm, with the lowest quantified values being below 5 ppm (e.g., in MW013 and MW025), and the higher values being greater than 149 ppm (e.g., in MW002 and MW007). The calculated Ce/Ce* for MW001 is 268.2. The Pr content varies from bdl to 7.8 ppm, with most values being ≤0.1 ppm. Within the MREE suite contents (in ppm): Nd ranges from bdl to 1020 ppm with most values being ≤2; Sm (0.02 to 38.0) is generally ≥1.6; Eu (0.06 to 14.0) is dominantly <1.0; whereas Gd (1.0 to 50.0) is mostly ≥9.0. The highest Nd value was obtained in MW006, which exceptionally has the highest Pr (7.8 ppm), Sm (37.1 ppm), and Eu (13.9 ppm) contents. The MW006 normalized chondrite plot in Figure 3a, shows positive Nd and Eu anomaly, not visible for other zircons. The calculated Eu/Eu* anomalies (0.05 to 2.1) and normalized chondrite plots (Figures 3 and 4) predominantly exhibit negative Eu anomalies with a few showing positive to the lack of an anomaly.

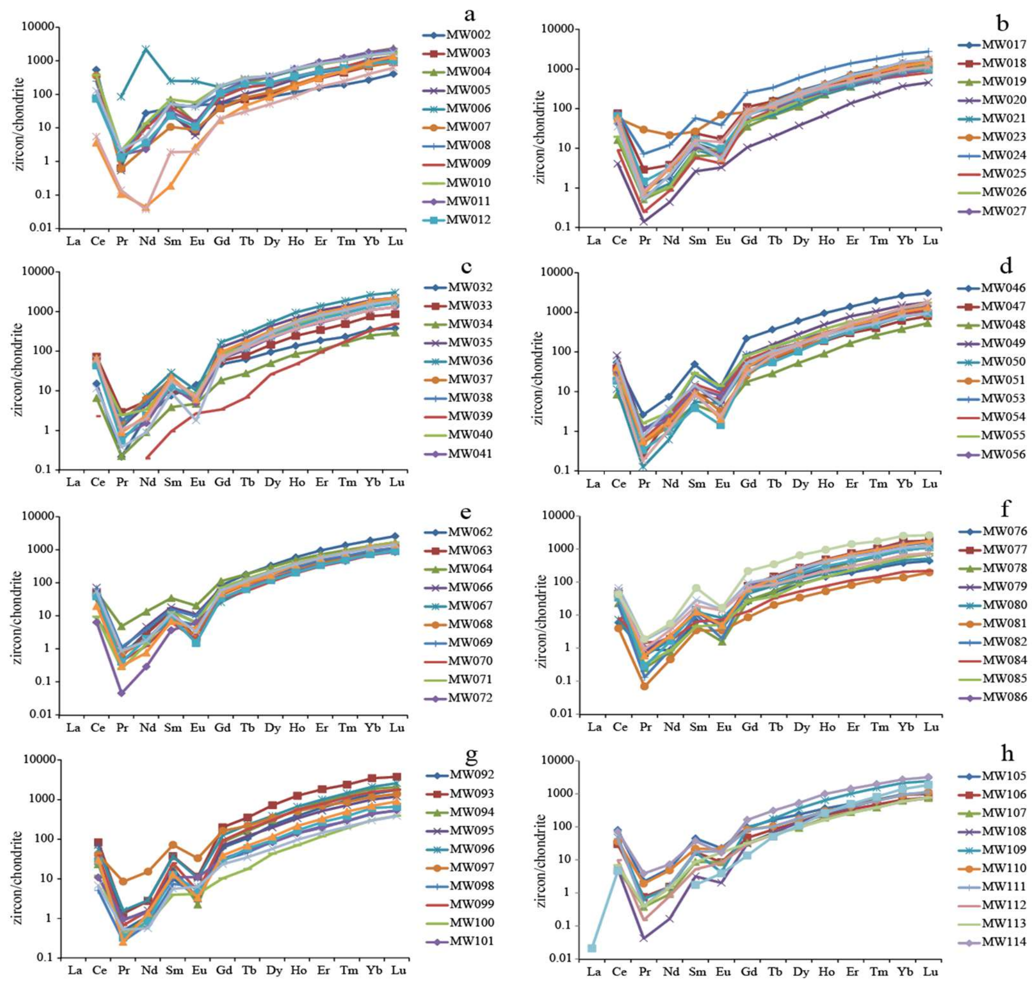

Figure 3. The western Meiganga magmatic zircon grains are normalized to [59] chondrite values and are plotted on Log_{10} versus element (La–Lu) diagrams.

Table 2. Rare earth element abundance (in ppm) in the western Meiganga detrital zircons.

Spot/Grain Number	La	Ce	Pr	Nd	Sm	Eu	Gd	Tb	Dy	Ho	Er	Tm	Yb	Lu	∑REE	Gd/Yb	Lu/Hf	Eu/Eu*	Ce/Ce*	Lu_n/Sm_n	Yb/Sm
MW001	0.01	14	0.031	0.3	1	0.65	6	2.3	36	18	106	27	287	69	567.83	0.022	0.0055	0.786	268.16	412.203	261.214
MW002	bdl	330	0.1	12.6	5.8	2.65	10	2.6	21	6	25	5	43	10	473.53	0.242	0.001	1.04	-	10.3625	6.815
MW003	bdl	bdl	0.1	bdl	3.6	0.45	8	2.5	25	9	48	11	110	22	238.698	0.07	0.002	0.261	-	37.117	27.986
MW004	bdl	bdl	0.1	bdl	10.3	0.79	22	7.6	78	30	130	29	286	58	652.058	0,078	0.0051	0.159	-	33.878	25.525
MW005	bdl	bdl	0.1	bdl	4.3	0.33	11	3.7	39	15	76	16	173	33	371.96	0.064	0.0027	0.146	-	46.591	36.984
MW006	bdl	bdl	7.8	1020	37.1	13.9	33	10.1	83	28	123	27	235	46	1663.24	0.138	0.0038	1.22	-	7.50816	5.823
MW007	bdl	218	0.1	1.2	1.6	0.5	8	2.9	28	11	54	12	113	23	472.896	0.067	0.0018	0.441	-	87.7531	66.163
MW008	bdl	151	0.1	5.3	7.7	2.35	21	5.7	53	17	69	14	139	26	511.547	0.15	0.0024	0.566	-	20.5491	16.582
MW009	bdl	202	0.1	4.5	6.4	0.85	16	5.7	49	18	80	17	161	30	590.589	0.097	0.0024	0.258	-	28.0132	23.154
MW010	bdl	230	0.2	6.2	10.4	3.23	35	11.4	87	30	125	25	229	42	833.157	0.152	0.0035	0.518	-	24.0651	20.206
MW011	bdl	49	0.1	1.1	4.5	0.79	23	9.2	84	32	147	31	288	54	722.845	0.079	0.0046	0.237	-	72.3288	58.832
MW012	bdl	45	0.1	1.7	3.4	0.62	21	7.5	54	18	77	15	132	24	401.475	0.161	0.0023	0.222	-	43.1254	35.903
MW013	bdl	2	0.01	0.02	0.028	0.15	3	1.6	20	9	49	12	147	33	278.568	0.023	0.0032	1.484	-	7176.54	4826.087
MW014	bdl	78	0.2	2.5	7.7	2.39	36	10.7	89	32	132	26	233	44	692.115	0.153	0.0038	0.44	-	34.3451	27.853
MW015	bdl	2	0.0049	bdl	0.1	0.2	1	0.6	10	3	1 8	4	49	11	100.8249	0.029	0.0009	2.074	-	1143.09	756.85
MW016	bdl	3	0.013	0.017	0.3	0.11	4	1.1	13	5	27	6	65	15	138.28	0.057	0.0013	0.331	-	325.952	211.757
MW017	bdl	26	0.1	0.9	2	0.44	15	5.9	69	23	117	25	226	43	553.821	0.068	0.0037	0.244	-	132.236	105.458
MW018	bdl	47	0.3	1.7	3.5	0.96	22	5.5	53	19	85	18	163	32	449.779	0.133	0.0025	0.335	-	53.9921	42.689
MW019	bdl	10	0.048	0.5	1	0.38	7	2.4	28	12	57	14	147	33	312.308	0.048	0.0027	0.449	-	210.252	142.243
MW020	bdl	3	0.013	0.2	0.4	0.19	2	0.7	9	4	22	6	59	11	116.636	0.036	0.0017	0.623	-	172.158	139.302
MW021	bdl	37	0.1	0.6	1.4	0.34	9	2.5	33	13	57	12	133	27	325.609	0.071	0.0024	0.288	-	118.113	89.898
MW022	bdl	2	0.005	bdl	0.2	0.46	4	1.7	32	16	108	30	339	71	604.555	0.01	0.0064	1.759	-	2356.37	1731.263
MW023	bdl	35	2.8	9.8	3.9	3.91	17	5.2	65	22	110	23	217	41	555.47	0.076	0.0031	1.482	-	62.4647	50.958
MW024	bdl	48	0.7	5.5	8.5	2.17	50	12.3	147	53	221	44	381	68	1040.33	0.131	0.006	0.322	-	47.9177	41.204
MW025	bdl	5	0.023	0.4	0.9	0.23	10	3.4	36	16	69	13	108	20	292.287	0.092	0.0016	0.244	-	138.514	115.655
MW026	bdl	12	0.1	0.5	1.3	0.53	9	3	48	14	65	13	126	23	303.886	0.073	0.0021	0.46	-	101.019	86.094
MW027	bdl	45	0.1	1.4	1.6	0.42	15	3.7	43	15	63	13	123	24	347.265	0.123	0.0022	0.265	-	91.2019	72.135
MW028	bdl	40	0.1	1.5	2.5	0.55	14	4.2	47	17	68	16	148	24	381.734	0.092	0.0022	0.29	-	59.6735	55.118
MW029	bdl	36	0.1	1.4	2	0.32	15	4.3	59	22	101	21	185	37	484.025	0.083	0.0035	0.176	-	112.203	85.169
MW030	bdl	21	0.049	1	2	0.3	13	4.9	62	22	112	24	241	43	545.699	0.054	0.0039	0.179	-	128.447	110.77
MW031	bdl	30	0.1	1.6	2.4	0.81	18	4.2	52	19	77	17	154	28	403.705	0.119	0.0026	0.375	-	70.6146	59.985
MW032	bdl	9	0.02	1.1	1.1	0.79	9	2.2	23	7	30	6	56	9	155.27	0.165	0.001	0.749	-	50.1355	46.542
MW033	bdl	44	0.3	2.5	1.5	0.38	11	2.8	36	13	54	12	122	21	320.877	0.093	0.0019	0.275	-	81.6493	72.764
MW034	bdl	4	0.021	0.4	0.6	0.27	4	1	12	5	17	4	40	7	94.806	0.092	0.0007	0.561	-	75.4671	64.025
MW035	bdl	31	0.1	2	3.2	0.31	25	7.7	105	37	170	34	306	54	776.26	0.082	0.0049	0.106	-	102.088	87.904
MW036	bdl	36	0.1	3.3	4.3	0.57	33	10.2	128	52	219	46	419	74	1026.421	0.079	0.0069	0.146	-	104.582	89.992
MW037	bdl	30	0.2	2.9	2.8	0.41	19	5.4	78	29	131	28	250	49	625.474	0.076	0.0046	0.169	-	103.685	81.462
MW038	bdl	27	0.2	2.3	2.8	0.35	17	5.1	68	26	120	25	234	46	573.706	0.072	0.0044	0.155	-	98.2727	76.55

Table 2. *Cont.*

Spot/Grain Number	La	Ce	Pr	Nd	Sm	Eu	Gd	Tb	Dy	Ho	Er	Tm	Yb	Lu	∑REE	Gd/Yb	Lu/Hf	Eu/Eu*	Ce/Ce*	Lu_n/Sm_n	Yb/Sm
MW039	bdl	1	bdl	0.1	0.1	0.15	1	0.2	6	3	15	4	54	12	96.543	0.013	0.0014	1.503	-	515.679	351.287
MW040	bdl	26	0.2	1.5	2.6	0.45	17	4.9	66	26	118	26	257	47	592.677	0.067	0.0046	0.204	-	107.791	89.488
MW041	bdl	28	0.1	0.7	1.9	0.27	13	4	52	20	84	18	171	32	428.857	0.072	0.0032	0.169	-	98.9272	82.875
MW042	bdl	27	0.1	1.1	1.9	0.38	14	4.4	60	23	106	22	211	40	510.261	0.066	0.0041	0.227	-	129.977	103.723
MW043	bdl	41	0.1	1.1	3.3	0.34	19	6.3	79	30	146	30	293	54	702.823	0.064	0.0048	0.132	-	98.9948	81.563
MW044	bdl	7	0.035	0.4	1.3	0.1	12	5.1	72	29	129	27	242	46	572.106	0.051	0.0041	0.076	-	207.875	166.22
MW045	bdl	37	0.1	0.9	2.6	0.41	14	4.4	55	20	89	18	175	32	449.417	0.08	0.0034	0.207	-	74.0463	61.873
MW046	bdl	33	0.2	3.4	7.2	0.74	43	13.1	148	52	220	48	421	75	1064.231	0.103	0.0076	0.128	-	62.5858	53.751
MW047	bdl	24	0.023	1	1.3	0.35	9	2.4	29	10	48	10	139	20	252.614	0.088	0.0022	0.315	-	89.113	68.08
MW048	bdl	5	0.1	0.6	0.7	0.15	3	1	13	5	26	6	140	13	135.353	0.058	0.0011	0.285	-	111.004	78.331
MW049	bdl	50	0.1	1.1	2.2	0.25	17	5.5	68	27	126	26	44	44	607.242	0.069	0.0044	0.124	-	119.781	100.245
MW050	bdl	7	0.0117	0.3	0.8	0.28	8	2.7	34	14	65	15	137	28	314.8147	0.06	0.0026	0.329	-	205.93	153.947
MW051	bdl	18	0.048	0.6	1.6	0.18	5	2.5	31	11	52	12	151	22	294.968	0.036	0.0022	0.195	-	82.2476	81.453
MW052	bdl	3	bdl	bdl	0.1	0.06	1	0.3	5	2	14	4	44	11	84.179	0.025	0.0012	0.545	-	634.716	399.876
MW053	bdl	18	0.1	1.3	4	0.62	17	4.7	52	16	74	14	137	25	364.86	0.126	0.0024	0.227	-	36.9077	31.498
MW054	bdl	33	0.1	1.1	2.3	0.52	13	4.1	41	17	72	16	151	27	376.477	0.083	0.0025	0.296	-	71.559	61.149
MW055	bdl	13	0.1	1.4	4.4	0.78	16	4.9	53	21	93	20	192	43	461.918	0.082	0,0047	0.287	-	59.3347	40.481
MW056	bdl	22	0.1	0.9	1.9	0.44	9	3	35	14	70	17	172	35	379.904	0.051	0.0034	0.334	-	113.821	85.366
MW057	bdl	12	0.031	0.5	0.6	0.08	6	2	25	11	53	12	124	24	270.042	0.05	0.0024	0.131	-	251.205	200.14
MW058	bdl	1	bdl	bdl	0.2	0.15	1	1.2	20	13	84	25	289	61	496.55	0.005	0.0056	0.965	-	2144.62	1562.733
MW059	bdl	25	0.1	0.8	1.4	0.11	8	3.6	40	16	74	16	165	32	381.926	0.049	0,0031	0.105	-	143.329	111.189
MW060	bdl	37	0.1	1.7	2.2	0.29	10	3.7	39	14	61	13	129	23	332.934	0.081	0.0023	0.184	-	64.3599	55.07
MW061	bdl	13	0.017	0.5	1.2	0.13	6	2.9	36	15	83	20	206	44	427.891	0.028	0.0044	0.153	-	213.259	153.956
MW062	bdl	25	0.1	1.5	2.1	0.35	17	6.5	81	32	152	34	306	63	719.894	0.054	0.0065	0.182	-	183.685	135.89
MW063	bdl	32	0.1	1.3	2	0.12	10	4	44	16	74	15	147	38	372.128	0.068	0.0029	0.083	-	82.0938	66.567
MW064	bdl	32	0.4	6.1	5.1	1.14	22	6.5	72	27	114	24	209	41	561.009	0.107	0.0041	0.326	-	48.7933	37.82
MW065	bdl	4	0.01	bdl	0.3	0.18	3	1.2	17	7	42	11	131	31	246.378	0.019	0.0026	0.681	-	738.797	482.425
MW066	bdl	44	0.1	2.1	2.7	0.62	14	4.5	43	15	68	13	128	22	356.051	0.108	0.0022	0.31	-	48.7563	43.639
MW067	bdl	5	0.1	0.8	1.1	0.3	5	2.3	29	13	57	12	117	22	263.702	0.043	0.0021	0.379	-	117.663	95.017
MW068	bdl	23	0.1	0.8	1.7	0.11	8	3.2	33	14	62	13	119	22	299.389	0.07	0.0023	0.093	-	76.8942	64.457
MW069	bdl	41	0.1	1.8	2.3	0.54	12	3.7	42	16	77	16	147	27	386.205	0.082	0.0028	0.313	-	71.5091	59.268
MW070	bdl	18	0.04	0.6	1	0.11	6	2	26	11	51	11	111	21	258.48	0.058	0.0023	0.136	-	134.256	107.311
MW071	bdl	6	0.023	0.6	1.9	0.37	14	4.7	56	21	99	21	211	41	476.01	0.066	0.0041	0.218	-	130.193	102.626
MW072	bdl	4	0.0042	0.1	0.5	0.35	7	2.5	32	12	56	11	120	21	264.7862	0.054	0.0022	0.56	-	234.23	203.768
MW073	bdl	24	0.038	0.9	1.3	0.09	7	2.3	30	11	54	12	116	23	280.683	0.059	0.0023	0.087	-	104.59	82.097
MW074	bdl	12	0.0276	0.4	1	0.23	10	3.5	42	19	90	20	192	36	425.9446	0.05	0.0037	0.222	-	212.058	174.749
MW075	bdl	34	0.1	0.8	1.7	0.19	12	4.1	52	20	91	20	178	35	448.726	0.065	0.0036	0.13	-	126.888	99.28
MW076	bdl	4	0.1	0.4	1	0.39	5	1.8	21	8	31	7	60	11	150.083	0.084	0.0012	0.544	-	67.7621	58.155
MW077	bdl	27	0.1	0.9	2	0.27	15	5.3	66	26	119	25	267	45	598.908	0.057	0.005	0.152	-	135.214	123.96
MW078	bdl	14	0.023	0.4	0.7	0.09	6	1.9	29	12	64	15	162	32	335.941	0.035	0.0034	0.136	-	275.889	212.742
MW079	bdl	32	0.1	0.9	1.8	0.23	9	3.4	38	15	69	15	143	28	354.659	0.061	0.0028	0.176	-	91.7397	72.829

Table 2. *Cont.*

Spot/Grain Number	La	Ce	Pr	Nd	Sm	Eu	Gd	Tb	Dy	Ho	Er	Tm	Yb	Lu	∑REE	Gd/Yb	Lu/Hf	Eu/Eu*	Ce/Ce*	Lu_n/Sm_n	Yb/Sm
MW080	bdl	4	0.1	0.8	1.9	0.46	9	2.8	29	10	39	7	74	12	191.144	0.12	0.0014	0.345	-	40.2054	36.523
MW081	bdl	2	0.0064	0.2	0.5	0.19	2	0.7	8	3	13	3	22	5	59.5164	0.077	0.0005	0.622	-	56.6236	39.654
MW082	bdl	12	0.0122	0.4	1.5	0.11	11	4.1	53	22	102	23	206	39	473.1912	0.053	0.0041	0.082	-	158.027	126.06
MW083	bdl	3	0.1	0.1	0.4	0.19	3	1.5	26	12	56	15	149	29	295.043	0.017	0.003	0.551	-	404.349	318.532
MW084	bdl	5	0.1	0.8	0.9	0.41	3	1.2	13	4	18	3	33	5	87.375	0.08	0.0006	0.799	-	34.3055	31.978
MW085	bdl	24	0.031	0.4	0.7	0.29	5	1.3	21	8	37	9	87	18	210.341	0.061	0.0022	0.468	-	157.141	119.229
MW086	bdl	24	0.1	1	2.2	0.26	15	4.8	64	25	113	24	231	42	545.592	0.066	0.0044	0.137	-	115.59	98.309
MW087	bdl	21	0.026	0.7	2.1	0.27	11	3.2	44	16	69	16	147	28	357.176	0.076	0.0031	0.168	-	77.3118	62.973
MW088	bdl	29	0.1	1.1	1.9	0.28	12	4.5	60	25	111	23	219	43	530.421	0.057	0,0045	0.174	-	136.006	107.083
MW089	bdl	41	0.2	2.1	4.2	0.83	19	4.8	63	23	93	18	175	30	472.53	0.107	0.0034	0.285	-	42.5854	38.255
MW090	bdl	25	0.1	1.6	2.8	0.77	13	3	33	12	48	10	104	19	272.28	0.125	0.0026	0.389	-	39.6817	33.999
MW091	bdl	26	0.2	2.5	9.8	0.93	43	12.5	158	51	224	42	402	64	1036.783	0.106	0.0069	0.139	-	39.1057	37.708
MW092	bdl	20	0.046	0.5	1.5	0.2	12	3.9	56	21	100	24	223	43	505.611	0.055	0.0047	0.138	-	172.918	135.453
MW093	bdl	51	0.1	1.3	5.6	0.64	40	12.7	177	68	291	59	555	92	1353.305	0.072	0.0101	0.131	-	100.054	91.925
MW094	bdl	14	0.038	0.5	2.9	0.13	17	5.8	75	31	143	32	298	51	669.605	0.057	0.0055	0.055	-	105.233	94.137
MW095	bdl	44	0.1	0.7	2.6	0.18	14	4.4	49	18	83	18	162	29	424.713	0.085	0.0032	0.091	-	67.7694	57.057
MW096	bdl	34	0.1	1.3	5.4	0.58	25	8.4	96	36	161	36	337	64	804.212	0.074	0.0065	0.153	-	70.8582	57.368
MW097	bdl	25	0.8	7	10.6	1.86	32	7.9	86	28	111	21	189	34	554.222	0.17	0.0045	0.307	-	19.3562	16.344
MW098	bdl	3	0.025	0.3	1.1	0.36	6	1.7	21	8	34	7	70	13	165.785	0.086	0.0014	0.427	-	71.6482	58.414
MW099	bdl	24	0.1	0.7	3.7	0.28	18	6.5	75	31	125	28	251	44	605.588	0.073	0.0044	0.102	-	71.2495	62.405
MW100	bdl	7	0.039	0.3	0.6	0.24	2	0.6	11	4	19	5	49	10	107.554	0.042	0.0013	0.651	-	97.6877	75.877
MW101	bdl	7	0.1	0.7	1.7	0.62	6	2	21	8	31	7	72	13	169.27	0.089	0.0014	0.583	-	47.7655	39.834
MW102	bdl	17	0.031	0.4	1.9	0.29	6	2.1	23	9	43	9	99	16	227.061	0.058	0.0016	0.272	-	52.1195	48.421
MW103	bdl	18	0.024	0.6	1.9	0.19	8	2.5	28	12	52	12	112	22	269.935	0.07	0.0027	0.151	-	69.9272	53.76
MW104	bdl	4	0.049	0.3	0.8	0.36	5	1.3	14	5	23	5	48	9	116.879	0.098	0.001	0.555	-	68.4259	53.051
MW105	bdl	49	0.2	2.5	6.6	1.27	19	5.8	58	20	80	16	156	26	439.665	0.123	0.0029	0.344	-	23.6093	21.658
MW106	bdl	18	0.1	0.7	2.6	0.48	9	3	35	12	54	12	106	19	271.97	0.088	0.002	0.3	-	44.6519	38.135
MW107	bdl	3	0.035	0.4	1.3	0.48	7	2.3	23	10	44	9	98	18	217.085	0.066	0.0019	0.507	-	85.5437	70.452
MW108	bdl	3	0.0039	0.1	0.5	0.11	6	2.4	34	14	64	16	150	24	313.8629	0.041	0.0021	0.205	-	308.493	293.379
MW109	bdl	29	0.1	0.7	2.5	0.24	18	6.3	89	35	161	37	345	60	781.979	0.051	0.0062	0.11	-	142.051	125.85
MW110	bdl	22	0.2	2.2	3.2	1.2	17	3.8	42	16	68	16	144	27	362.808	0.116	0.0032	0.499	-	50.5069	40.771
MW111	bdl	27	0.037	0.8	2.6	1.03	16	3.7	45	15	68	15	151	28	374.017	0.106	0.0031	0.486	-	65.7375	53.665
MW112	bdl	6	0.014	0.4	0.8	0.46	6	2.1	24	9	43	10	93	19	213.594	0.064	0.0019	0.652	-	144.547	111.266
MW113	bdl	4	0.037	0.7	1.3	0.94	6	2.1	24	9	42	9	95	19	213.517	0.066	0.0027	1.005	-	88.6116	67.697
MW114	bdl	43	0.4	3.4	5.5	0.92	32	11.1	131	54	228	49	436	79	1073.568	0.074	0.0078	0.21	-	86.1966	72.872
MW115	0.01	3	bdl	bld	0.3	0.22	3	1.8	27	14	79	20	224	46	417.615	0.012	0.0044	0.8	-	1052.85	791.973

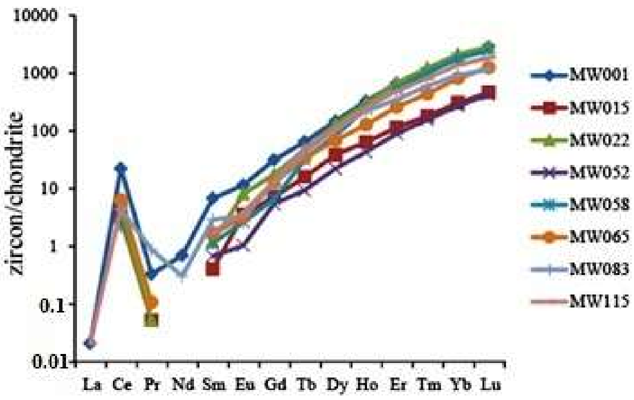

Figure 4. The western Meiganga metamorphic zircon grains are normalized to [59] chondrite values and are plotted on Log_{10} versus element (La–Lu) diagrams.

Heavy rare earth elements are mainly the highest in zircons from the western Meiganga gold placer. High HREE contents are common in zircon, as these REEs mainly substitute Zr in zircon structure [27]. Within this group of REE, Yb (22 to 555 ppm) and Er (12 to 222 ppm) contents are generally the highest, whereas those of Ho (2 to 53 ppm), Tm (3 to 48 ppm), and Tb (0.7 to 13.1 ppm) are the lowest. The Dy contents (6 to 148 ppm, with most values exceeding 30 ppm) and that of Lu (5 to 74 ppm; with most values exceeding 20 ppm) are moderately high. The calculated Gd/Yb and Lu/Hf ratios range from 0.01 to 0.25 and 0.0005 to 0.010, respectively. The highest Gd/Yb (≈0.24) and Lu/Hf (≈0.010) ratio was respectively obtained in MW002 and MW093; with MW093 having the highest Lu (92 ppm), Yb (555 ppm), Tm (59 ppm), Er (291 ppm), and Ho (177 ppm) contents. The calculated Lu_n/Sm_n ratios range from 7 to 7177 and that of Yb/Sm, from 20 to 4827. Except for MW013 (with Th/U ≈ 0.4, Lu_n/Sm_n ≈ 7176.5, Yb/Sm ≈ 4827), the highest values were mainly obtained for zircon with Th/U < 0.07.

4.2. U–Pb Dating

The $^{206}Pb/^{238}U$ (575 to 2927 Ma, dominantly ≥1900 Ma, Figures 5 and 6) and $^{207}Pb/^{206}Pb$ (565 to 3088 Ma; dominantly >2000 Ma) dates are highly heterogeneous, with some zircons having the same age (Table 3). Due to this high heterogeneity, the $^{206}Pb/^{238}U$ ages are used to group the zircons into six sets: (1) Neoproterozoic (575 to 834 Ma); (2) Late-Mesoproterozoic (986–1162 Ma); (3) Late Paleoproterozoic (1643–1996 Ma); (4) Early Paleoproterozoic (2003–2490 Ma); (5) Neoarchean (2789–2500 Ma); and (6) Meso-archean (≥2907 Ma). Late Paleoproterozoic zircons are proportionally the highest, whereas Late Mesoproterozic and Meso-archean zircons are the lowest.

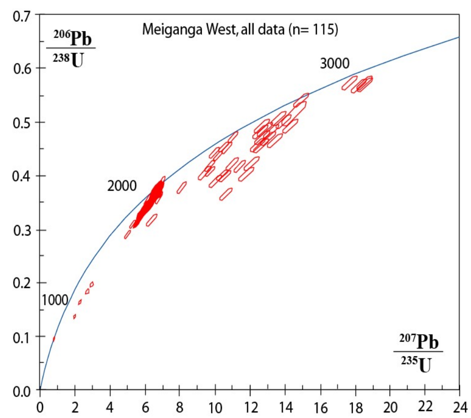

Figure 5. U–Pb discordia diagram for the western Meiganga detrital zircons.

Table 3. Isotopic geochemical data and U–Pb core age (in Ma) for the west Meiganga detrital zircons.

Spot/Grain Number	$^{207}Pb/^{206}Pb$	2 s %	$^{207}Pb/^{235}U$	2 s %	$^{206}Pb/^{238}U$	2 s %	$^{207}Pb/^{206}Pb$ Age	2 s. Abs.	$^{207}Pb/^{235}U$ Age	2 s. Abs.	$^{206}Pb/^{238}U$ Age	2 s. Abs.	% of Age Discordance
MW001	0.05898	1.0559297	0.8097	2.2135129	0.0994	1.9454181	568	6	602	13	611	12	7.57
MW002	0.18773	1.0258972	12.658	1.9851962	0.4885	1.6995702	2722	17	2654	53	2564	44	−5.81
MW003	0.12681	1.096377	6.45	2.1813458	0.3707	1.8857961	2054	19	2039	44	2033	38	−1.02
MW004	0.12885	1.0171991	6.573	2.0606938	0.3716	1.7921398	2082	18	2056	42	2037	37	−2.16
MW005	0.12828	1.0159463	6.525	2.0605022	0.3711	1.7926301	2075	18	2049	42	2035	36	−1.93
MW006	0.10719	1.0227616	2.728	2.3930905	0.1854	2.1635251	1752	19	1336	32	1096	24	−37.44
MW007	0.17303	1.0332651	9.676	2.0501816	0.4086	1.7707647	2587	17	2404	49	2210	39	−14.57
MW008	0.17358	1.0095133	10.676	2.0531525	0.4513	1.787825	2593	17	2495	51	2401	43	−7.41
MW009	0.12967	1.0230479	6.159	2.1094446	0.3485	1.8447574	2094	18	1998	42	1927	36	−7.97
MW010	0.12733	1.0238928	5.678	2.0718654	0.3264	1.8011856	2062	18	1928	40	1821	33	−11.69
MW011	0.12849	1.0202675	6.231	2.1145741	0.3537	1.8521549	2077	18	2009	42	1952	36	−6.02
MW012	0.20117	1.0215618	14.87	2.0797817	0.5414	1.8116025	2836	17	2807	58	2789	51	−1.66
MW013	0.1973	1.1449174	12.84	3.0424281	0.474	2.8187822	2803	19	2664	81	2500	70	−10.81
MW014	0.12947	1.0400339	6.085	2.1790844	0.3422	1.914873	2091	18	1988	43	1900	36	−9.13
MW015	0.12915	1.018563	6.14	2.5696011	0.3461	2.3591056	2087	18	1995	51	1915	45	−8.24
MW016	0.19232	1.0214002	12.96	2.4406119	0.4889	2.2166028	2762	17	2676	65	2570	57	−6.95
MW017	0.12961	1.0420935	6.387	2.1452971	0.3579	1.8751909	2093	18	2030	44	1972	37	−5.78
MW018	0.12725	1.0311348	5.672	2.1894708	0.3235	1.9314615	2060	18	1927	42	1807	35	−12.38
MW019	0.1694	1.0377757	10.174	2.1352802	0.4373	1.8661305	2552	17	2451	52	2338	44	−8.39
MW020	0,1952	1.0228859	13.58	2.0498205	0.5054	1.7763638	2787	17	2721	56	2637	47	−5.38
MW021	0.12872	1.0426656	6.031	2.0164531	0.3399	1.7259581	2080	18	1980	40	1886	33	−9.33
MW022	0.05992	1.1259031	0.7865	2.0793247	0.09514	1.7481228	602	24	589	12	586	10	−3.32
MW023	0.10314	1.1199047	1.96	2.3889438	0.1381	2.1101815	1681	21	1101	26	834	18	−50.39
MW024	0.10827	1.0598033	2.942	2.1245751	0.1975	1.841368	1771	19	1393	30	1162	21	−34.39
MW025	0.1294	1.0537672	6.685	2.066182	0.3748	1.7772684	2090	19	2071	43	2054	37	−1.72
MW026	0,16279	1.0790615	9.917	2.0173669	0.4424	1.704522	2486	18	2427	49	2363	40	−4.95
MW027	0.12683	1.0416841	5.461	2.3922151	0.3122	2.1535058	2055	18	1894	45	1751	38	−14.79
MW028	0.12969	1.0584876	6.208	1.9730388	0.3471	1.6650784	2094	19	2006	40	1921	32	−8.26
MW029	0.13105	1.0312174	6.577	2.1198996	0.3644	1.8521784	2112	18	2056	44	2003	37	−5.16
MW030	0.13119	1.0523462	6.671	2.0503635	0.3686	1.759704	2114	18	2069	42	2023	36	−4.31
MW031	0.12494	1.0214233	4.994	2.129226	0.2903	1.8682339	2028	18	1818	39	1643	31	−18.98
MW032	0.20088	1.0763834	13.942	2.0184594	0.5031	1.7075061	2833	18	2746	55	2627	45	−7.27
MW033	0.12819	1.0499029	5.576	2.1349278	0.317	1.8589299	2073	18	1913	41	1775	33	−14.38
MW034	0,1914	1.1802872	10.55	2.0383995	0.4005	1.661925	2754	19	2485	51	2171	36	−21.17
MW035	0.12953	1.0561198	6.958	2.0058773	0.3898	1.7053312	2092	19	2106	42	2122	36	1.34
MW036	0.13349	1.0652415	6,751	2.1104932	0.3672	1.8219336	2144	19	2079	44	2016	37	−5.97
MW037	0.13003	1.0769987	6.395	2.0082954	0.3573	1.6950883	2098	19	2032	41	1969	33	−6.15
MW038	0.13165	1.0592867	6.573	2.1741149	0.362	1.8986014	2120	19	2056	45	1992	38	−6.04
MW039	0.1987	1.0490603	12.729	2,144,827	0.4642	1.8707633	2816	17	2660	57	2458	46	−12.71
MW040	0.1299	1.0419095	6.519	2.0785535	0.3652	1.7985575	2097	18	2048	43	2006	36	−4.34
MW041	0.19553	1.0416243	13.65	2.022665	0.509	1.7338375	2789	17	2726	55	2652	46	−4.91

Table 3. *Cont.*

Spot/Grain Number	$^{207}Pb/^{206}Pb$	2 s %	$^{207}Pb/^{235}U$	2 s %	$^{206}Pb/^{238}U$	2 s %	$^{207}Pb/^{206}Pb$ Age	2 s. Abs.	$^{207}Pb/^{235}U$ Age	2 s. Abs.	$^{206}Pb/^{238}U$ Age	2 s. Abs.	% of Age Discordance
MW042	0.12926	1.0283564	6.244	2.24707	0.351	1.9979506	2088	18	2010	45	1939	39	−7.14
MW043	0.13249	1.058558	6.603	2.2262665	0.363	1.9584988	2131	19	2060	46	1996	39	−6.34
MW044	0.13109	1.041167	6.271	2.1850543	0.348	1.9210501	2113	18	2014	44	1925	37	−8.90
MW045	0.1299	1.0298956	6.432	2.087899	0.3607	1.816215	2097	18	2037	43	1985	36	−5.34
MW046	0.13272	1.0444299	6.803	2.1382101	0.3751	1.8657729	2134	18	2086	45	2053	38	−3.80
MW047	0.12917	1.0641406	6.633	2.0708768	0.3756	1.7765515	2087	19	2064	43	2056	37	−1.49
MW048	0.15565	1.0483819	8.07	2.2663001	0.3785	2.0092316	2409	18	2238	51	2069	42	−14.11
MW049	0.12891	1.0382624	6.724	2.0252126	0.3819	1.7388207	2083	18	2076	42	2085	36	0.10
MW050	0.19019	1.0264121	12.5	2.1569862	0.4807	1.8971209	2744	17	2642	57	2530	48	−7.80
MW051	0.12922	1.0961129	6.2	2.0578893	0.3488	1.7416788	2087	19	2004	41	1929	34	−7.57
MW052	0.05891	1.1899966	0.762	2.1652317	0.0948	1.8089048	565	26	575	12	584	11	3.36
MW053	0.12455	1.0249582	5.296	2.2430844	0.3104	1.9952164	2022	18	1868	42	1742	35	−13.84
MW054	0.21068	1.0679921	13.39	2.3038529	0.4654	2.0413552	2911	17	2709	62	2463	50	−15.39
MW055	0.20151	1.0433869	13.63	2.3187192	0.4945	2.070701	2838	17	2726	63	2590	54	−8.74
MW056	0.10087	1.0721416	2.283	2.2745103	0.1653	2.0059685	1640	20	1207	27	986	20	−39.88
MW057	0.12904	1.066943	6.496	2.0585324	0.3677	1.7604511	2085	19	2045	42	2018	36	−3.21
MW058	0.05871	1.0739985	0.7891	2.1348847	0.09795	1.8450636	556	23	591	13	602	11	8.27
MW059	0.12714	1.0393148	6.028	2.2327585	0.3449	1.9761161	2059	18	1979	44	1910	38	−7.24
MW060	0.12964	1.0511704	6.281	2.2103342	0.353	1.9443812	2093	18	2016	45	1948	38	−6.92
MW061	0.17004	1.0344256	11.002	2.1131229	0.4705	1.842621	2558	17	2524	53	2485	46	−2.85
MW062	0.13171	1.0256123	6.816	2.1905211	0.3764	1.9355883	2121	18	2087	46	2059	40	−2.92
MW063	0.13171	1.0567551	6.196	2.3090997	0.342	2.0530977	2121	19	2003	46	1896	39	−10.61
MW064	0.13266	1.1070358	6.376	2.2014806	0.3495	1.9028895	2133	19	2029	45	1932	37	−9.42
MW065	0.05927	1.2354517	0.7635	2.1669145	0.09353	1.7802184	579	27	576	12	576	10	−0.52
MW066	0.13113	1.0258365	6.426	2.0775316	0.3576	1.8065982	2113	18	2037	42	1971	36	−6.72
MW067	0.18913	1.1029476	10.947	2.2642112	0.4217	1.9774122	2734	18	2518	57	2268	45	−17.04
MW068	0.12784	1.0388935	6.549	2.1619099	0.3736	1.8959311	2068	18	2052	44	2046	39	−1.06
MW069	0.12983	1.0377318	6.531	2.1316465	0.3675	1.8619961	2097	18	2050	44	2017	38	−3.81
MW070	0.12849	1.0428153	6.57	1.9981856	0.3744	1.7044887	2077	18	2055	41	2050	35	−1.30
MW071	0.19883	1.0997584	11.387	2.1970896	0.4181	1.9020342	2816	18	2555	56	2251	43	−20.07
MW072	0.19584	1.074518	12.611	2.1231418	0.4716	1.8311587	2792	18	2651	56	2490	46	−10.82
MW073	0.12709	1.0507496	5.729	2.2149697	0.332	1.949876	2058	19	1935	43	1848	36	−10.21
MW074	0.12982	1.024647	6.129	2.1942416	0.3462	1.9403079	2096	18	1994	44	1916	37	−8.59
MW075	0.12819	1.0326037	5.779	2.225006	0,3302	1.9708834	2073	18	1943	43	1839	36	−11.29
MW076	0.2085	1.3210992	12.02	2.9420867	0,4219	2.6287966	2893	21	2606	77	2269	60	−21.57
MW077	0.13258	1.0467253	6.831	2.3109462	0,3775	2.0603006	2132	18	2089	48	2064	43	−3.19
MW078	0.12706	1.0393634	6.2	2.2252813	0,358	1.9676384	2058	18	2004	45	1972	39	−4.18
MW079	0.13043	1.0505673	6.53	2.3194624	0,3664	2.067901	2105	18	2049	48	2012	42	−4.42
MW080	0.212	1.3118297	11.82	3.4037478	0,407	3.1407964	2920	21	2589	88	2200	69	−24.66
MW081	0.16841	1.0431425	9.35	2.5602847	0,4047	2.3381427	2542	17	2372	61	2190	51	−13.85
MW082	0.13304	1.1032586	6.43	2.2902349	0.3549	2.0069868	2139	19	2036	47	1958	39	−8.46
MW083	0.06028	1.0763443	0.7995	2.3507088	0.0967	2.0898121	614	23	596	14	595	12	−3.09
MW084	0.18666	1.0410054	10	2.6694281	0.3912	2.4580794	2713	17	2433	65	2127	52	−21.60
MW085	0.12958	1.0488629	6.728	2.3527961	0.3797	2.1060713	2092	18	2078	49	2074	44	−0.86
MW086	0.12773	1.0309047	5.872	2.3127691	0.3349	2.0702986	2067	18	1956	45	1862	39	−9.92

Table 3. *Cont.*

Spot/Grain Number	$^{207}Pb/^{206}Pb$	2 s %	$^{207}Pb/^{235}U$	2 s %	$^{206}Pb/^{238}U$	2 s %	$^{207}Pb/^{206}Pb$ Age	2 s. Abs.	$^{207}Pb/^{235}U$ Age	2 s. Abs.	$^{206}Pb/^{238}U$ Age	2 s. Abs.	% of Age Discordance
MW087	0.12985	1.051009	6.684	2.2446378	0.3754	1.9833756	2096	18	2070	46	2055	41	−1.95
MW088	0.12813	1.0475964	6.556	2.399084	0.3728	2.1582739	2072	18	2052	49	2042	44	−1.44
MW089	0.12837	1.0649181	5.639	2.5845292	0.3183	2.3549397	2076	19	1921	50	1781	42	−14.21
MW090	0.23299	1.0274848	18.3	2.460428	0.57	2.2356165	3073	16	3004	74	2907	65	−5.40
MW091	0.13246	1.0715605	6.767	2.307766	0.3697	2.0435769	2131	19	2081	48	2031	42	−4.69
MW092	0.12723	1.0744489	5.612	2.3350095	0.3186	2.0731206	2060	19	1919	45	1782	37	−13.50
MW093	0.2099	1.1289986	14.27	2.4068045	0.4931	2.1255752	2904	18	2767	67	2583	55	−11.05
MW094	0.13098	1.075925	6.128	2.4087246	0.3394	2.155073	2111	19	1994	48	1883	41	−10.80
MW095	0.13068	1.094069	6.17	2.3231052	0.3436	2.0493489	2107	19	2000	46	1904	39	−9.64
MW096	0.1451	1.8162735	6.38	3.338447	0.3175	2.8011388	2288	31	2030	68	1777	50	−22.33
MW097	0.16682	1.0422462	10.421	2.085877	0.4527	1.806822	2526	17	2473	52	2407	43	−4.71
MW098	0.19947	1.0991481	12.98	2.27661	0.4708	1.9936967	2822	18	2678	61	2487	50	−11.87
MW099	0.13511	1.1621508	6.741	2.2536652	0.3608	1.9309097	2165	20	2079	47	1986	38	−8.27
MW100	0.2042	1.5807864	14.53	3.5242336	0.516	3.1498153	2859	26	2783	98	2680	84	−6.26
MW101	0.19786	1.049468	12.52	2.1522679	0.4567	1.8790621	2809	17	2644	57	2425	46	−13.67
MW102	0.12944	1.0537348	6.327	2.096248	0.3526	1.8121531	2090	19	2022	42	1947	35	−6.84
MW103	0.12946	1.0561789	6.687	2.0679553	0.3741	1.7778992	2091	19	2071	43	2049	36	−2.01
MW104	0.18647	1.0839618	10.367	2.1415732	0.401	1.8469875	2711	18	2468	53	2173	40	−19.85
MW105	0.13103	1.0905219	6.291	2.1442284	0.3474	1.8462062	2112	19	2018	43	1922	35	−8.99
MW106	0.12864	1.0620115	5.895	1.9959839	0.3308	1.6899951	2079	19	1960	39	1842	31	−11.40
MW107	0.1957	1.1730277	12.388	2.1421758	0.4579	1.7924629	2791	19	2634	56	2433	44	−12.83
MW108	0.18535	1.0207998	12.651	2.0261364	0.4934	1.7501991	2702	17	2655	54	2585	45	−4.33
MW109	0.13297	1.0683607	6.661	2.0837709	0.3623	1.7890519	2137	19	2068	43	1993	36	−6.74
MW110	0.2353	1.0816384	18.51	2.0484036	0.5713	1.7395447	3088	17	3017	62	2913	51	−5.67
MW111	0.20941	1.0402371	10.59	2.3474282	0.3658	2.1043588	2901	17	2487	58	2009	42	−30.75
MW112	0.16789	1.0308161	9.68	2.1739041	0.4189	1.913969	2537	17	2406	52	2255	43	−11.12
MW113	0.22314	1.0480508	17.66	2.0670773	0.5741	1.7816841	3003	17	2971	61	2927	52	−2.53
MW114	0.13297	1.0533261	6.694	2.0342353	0.3652	1.7402924	2137	18	2072	42	2007	35	−6.08
MW115	0.06006	1.1923323	0.7893	2.0599996	0.09574	1.6798637	607	26	591	1	589	10	−2.96

2 s %: isoplot error in percentage; 2 s. abs: absolut isoplot error; % of age discordance = ($^{206}Pb/^{238}U$ age/$^{207}Pb/^{206}Pb$ age − 1) × 100.

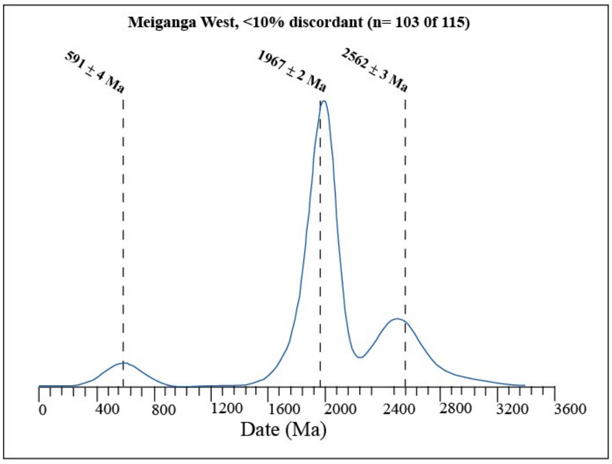

Figure 6. Plot showing spatial distribution of U–Pb ages for the western Meiganga detrital zircons.

5. Discussion

Geochemical and U–Pb geochronological results are used to characterize each zircon grain and to understand its genetic history. They are correlated with rocks within the local and regional setting in order to locate their primary source (s).

5.1. Geochemical Characterization Vis-Vis-Source and Genetic Constraints on Zircon

5.1.1. Geochemistry of Zircon and Possible Magmatic Segregation

Uranium, Th, Hf, Y, and REE contents are commonly used to characterize zircons and understand the history of their genesis [27,57,58,60,61]. Heaman et al. [27] demonstrated that zircon chemistry can reflect the composition of the magma from which it is crystallized and its tectonic setting. Out of 115 zircon grains, a total of nine trace elements and REEs are highly heterogeneous with equal values found in some. The heterogeneity in elemental contents suggests that the zircons were crystallized in different rock types with some of the sources being more chemically enriched than others. The equal elemental contents found in some of the zircons may relate their crystallization to an environment with the same abundance of these elements.

The Th/U of Meiganga zircons fall within the reported envelope for zircons of both igneous [54,58,61] and metamorphic [57] origins. Three main groups distinguished are: (1) magmatic zircons (Th/U $\geq$ 0.2); (2) metamorphic affiliated zircons (Th/U < 0.07); and (3) grains with Th/U ratios ranging from 0.09 to < 0.2. The highest Th/U ratios (>1.0) obtained in some of the group 1 zircons could suggest preferential incorporation of Th into those zircon lattices over U, or relate the crystallization of their source under amphibolite or eclogite melting conditions [62]. The nature of zircons in group 3 is not easy to determine. They may be metamorphic zircons, with high Th/U [60], originating from high-grade metamorphic rocks (e.g., [63]). In this study, a grain with Th/U ($\approx$0.09) is considered metamorphic as its other features are similar to those of metamorphic zircons in group 3. Those with Th/U ratios (>0.09) and (<0.2), quite close to magmatic grains, were affiliated to magmatic zircons in group 1. They may be zircons from partial melt segregation, as their Th/U ratios are within the range (0.13–0.37) in some partial melt segregation zircons studied by [64]. The partial-melt segregation origin of those grains (MW067, MW081, MW082, and MW108) is supported by Ti thermometric data (618 $\pm$ 87 to 744 $\pm$ 66 °C), which are similar to those obtained by [64] for zircon that grew by partial melt segregation process. The other features that characterize those grains is their position within various plots, situated out of various fields in Y versus U, Y versus Nb/Ta, and Y versus Yb/Sm binary diagrams (Figures 7–9). The significant variation in Y (81–626 ppm), U (115–442 ppm), Th (23–169 ppm), Pb (30–158 ppm), and $\sum$REE (59–474 ppm) contents in those zircons suggests crystallization in different environments with these environments being Y, U, Th, and REE are enriched than others. The Hf abundance (9430–11,460 ppm) is greater than values (<9000 ppm: [27]) in zircons formed during continental rifting. The Eu/Eu* (0.08–0.63), their large positive and negative Ce anomalies (Figure 3e,f,h) and chondrite-normalized REE patterns are close to that of magmatic zircons, which helps to classify them as magmatic. These may also represent zircon that crystallized in anatectic melts, as their geochemical features are similar to those of anatectic zircons.

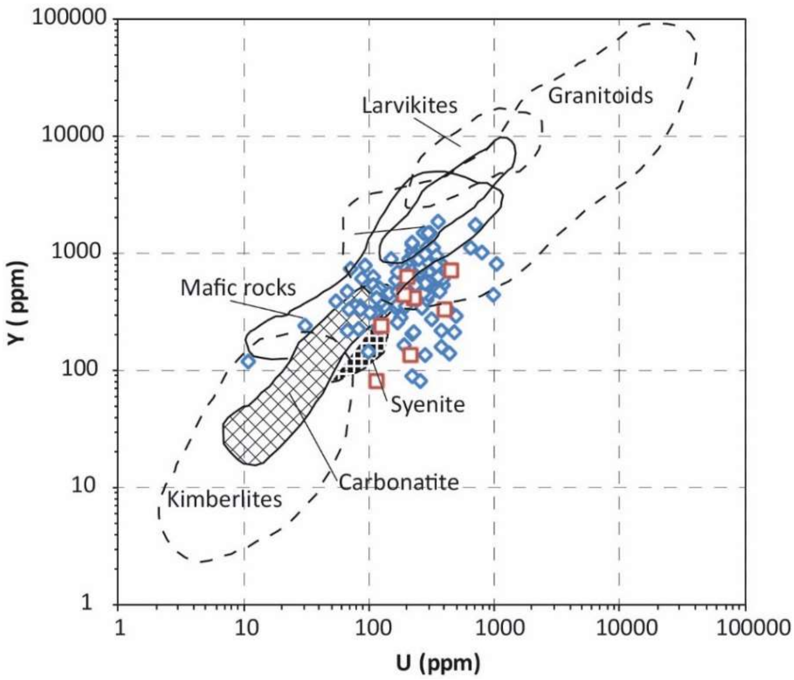

Figure 7. Y versus U plot of western Meiganga magmatic zircons (adapted from [19,54], blue and white diamond-shape plots are for magmatic zircons; red and white square plots are for metamorphic zircon).

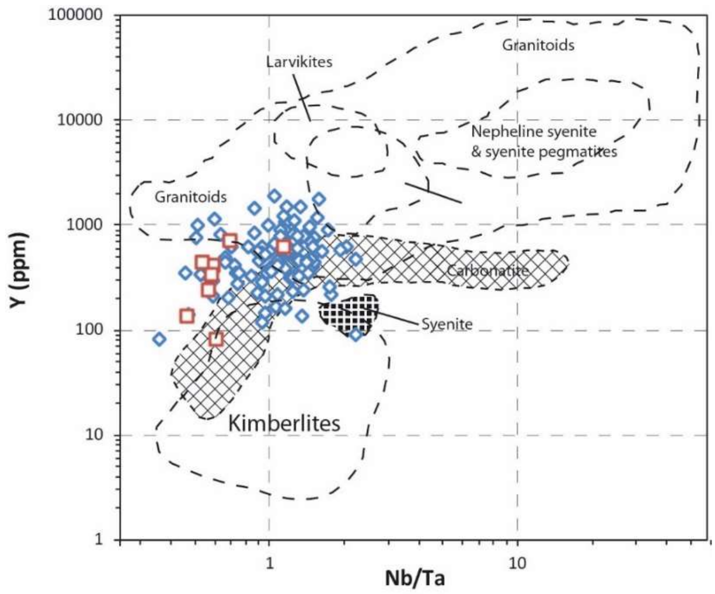

Figure 8. Y versus Nb/Ta plot of western Meiganga magmatic zircons (adapted from [19,54], blue and white diamond-shape plots are for magmatic zircons; red and white square plots are for metamorphic zircon).

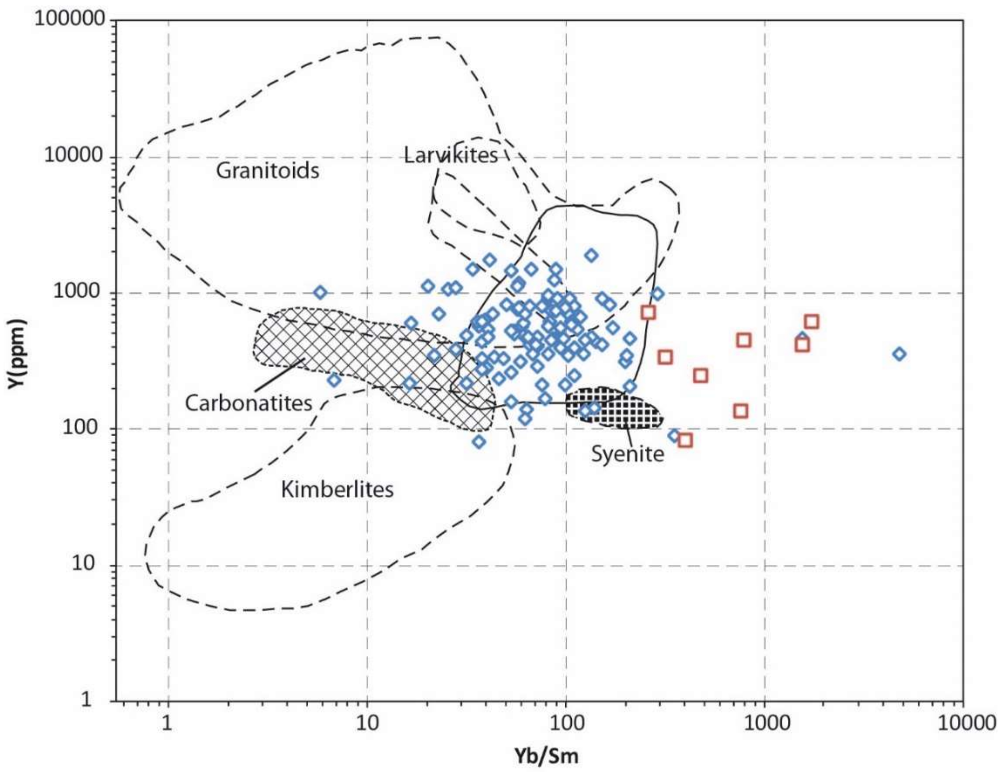

Figure 9. Y versus Y/Sm plot of western Meiganga magmatic zircons (adapted from [19,54], blue and white diamond-shape plots are for magmatic zircons; red and white square plots are for metamorphic zircon).

Magmatic Affiliated Zircons

The variable Hf contents (6390–13,020 ppm) in the western Meiganga magmatic zircons, suggest a different degree of Hf substitution in the zircon lattice. The same interpretation is consistent for the U, Th, and Y contents, as they also show consistent variations. The Pb (42–629 ppm), Ti (2–133 ppm), Nb (0.2–7.0 ppm), and Ta (0.2–8.0 ppm) contents in the zircons, are significantly low to very low. The presence of relatively-high Pb concentrations (e.g., 618 ppm: MW036; 629 ppm: MW093) in some of these zircons may be due to high concentration of this element in source magma coupled with Pb from Th and U radiogenic decay [65]; In contrast, the very low Pb content may be due loss of radiogenic Pb by diffusion during the geological history of low-Pb zircon source rock (cf. [66–69]. Titanium does not frequently substitute for Zr in the zircon structure and the concentration is temperature dependent [70,71]. The low Ti in most of the zircons may be due of low degree of Ti substitution, and the absence of favorable temperature for its maximum concentration in those zircons. The relative high Ti content found in MW048 (Ti: 133 ppm) differentiates this zircon from others and relates its crystallization to a Ti-enriched environment, with significantly high temperature to facilitate Ti substitution in its structure.

The very low to low Nb and Ta contents in the western Meiganga zircons are probably due to the fact that these two elements do not easily substitute into the zircon structure. The highest Nb (6.9 ppm) and Ta (7.8 ppm) in some of those zircons can be explained by Nb, Ta, and REE coupled substitutions {$(Y, REE)^{3+} + (Nb, Ta)^{5+} \leftrightarrow 2\ Zr^{4+}$: [65]}, as those grains also have the highest ∑REE values. As shown in Figure 2d, there is a positive correlation between Nb and Ta showing that the degree of Nb and Ta substitution is the same, as most obtained Nb values are close to those of Ta.

The studied zircons are mostly REE enriched, as the ∑REE (generally below 800 ppm) are below those obtained ∑REE (up to 2161 ppm) in the Western Mamfe clastic zircons as studied by [12]. Within the REE suites, particular features were noted: the absence of La, extreme variation of Ce contents, high Nd in MW006 and Eu anomaly. The Zr^{4+} radius (0.84 Å) is close and matched the smaller HREE radii than larger LREE (e.g., La^{3+}: 1.60 Å) such that the LREE are generally incompatible in the zircon structure [65]. The absence of La in the western Meiganga magmatic zircons may be due to the non-substitution of this element in their lattice, whereas the extreme variation of Ce abundance can be interpreted differently. For example, the below detection of Ce contents in part of the zircons may typify the lack of substitution of Ce and the presence of Ce^{3+} (incompatible in zircon structure) and very low oxidization state in the source magma [65]. The low Ce (1–18 ppm) and relatively high (150–330 ppm) contents found in some zircons are due to different oxidation state of Ce substitution in those grains. The low recorded Ce value can be due to limited Ce^{4+} concentrations (low oxidization condition) in their source magma, whereas the relatively high values may typify high Ce^{4+}concentration (high oxidization state) [72].

The calculated Eu anomalies range from 0.08 to 1.8 with most of those values being below 1 (negative anomalies), indicating reducing condition. The Nd content (1020 ppm in MW006) is the highest obtained value for REE in the studied zircons. This feature differentiates the grain from others, as it also encloses the highest Pr, Sm, and Eu (positive anomaly: Figure 3a). It is difficult to discern a particular interpretation to this feature as data on fluid/melt and mineral inclusions are absent. The very pronounced Eu negative anomalies ($Eu/Eu^* \leq 0.1$) for the magmatic zircons, characterize reducing conditions and may reflect a crystallization of a mantle source magma as the Eu anomalies in this magma are very low [65]. The low negative Eu anomaly ($0.1 < Eu/Eu^* < 1$; reducing condition) and relatively high positive Eu anomalies: $Eu/Eu^* = 1$(no anomaly), and $Eu/Eu^* > 1$ (positive anomaly: oxidizing condition) are the dominant features found in magmatic zircons that grew within the crust.

Source and Tectonic Frame Work

Hafnium, U, Th, Y, Ti, and REE abundances in zircons have been used to study the tectonic setting and identified a specific source rock type [19,27,73,74]. Heaman et al. [27] described the Hf content in zircons crystallized within a continental rift setting as below 9000 ppm. Hafnium contents in the western Meiganga detrital zircons are predominantly >9000 ppm; with part of the zircons grew during continental rifting. For [74] the Hf content in some zircons from oceanic crust is greater than 1.1 wt %. The Hf contents in part of the studied Hf-enriched zircons are within the range limit noted by [74] in oceanic crust zircons. However, it is not easy to associate the crystallization of these zircons (Hf > 10,000 ppm) to an oceanic crust setting, as some analyses/works are still needed to unequivocally support this hypothesis. Hafnium contents in zircons from alkaline magmatic rocks are below 11 wt % (e.g., [19,54]).

Element contents in part of the studied zircons are within the range limit in alkaline magmatic zircons; relating their crystallization in alkaline rocks. The group 1 ($Hf \leq 8910$ ppm) are within the range (6000–8000 ppm) in nepheline-syenite zircons of [27], higher than the value (Hf = 5900 ppm) in syenites studied by [63]. Relating their crystallization to nepheline syenite is not possible, as they were not plotted in nepheline syenite field in any of the three diagrams in Figures 7–9, but in kimberlite, syenite, granitoid, or mafic rocks. Those greater than 9000 ppm, are within the range in zircons from mafic rocks [27], dolerites [54], and some gabbro [74]. Those in group 3 ($Hf \geq 10{,}000$ ppm) are within the range (dominantly within 10,065 and 12,981 ppm) in zircons from felsic rocks studied by [27], with some of those values close to those in zircons from [54]. The granitoid affiliation of some of those zircons is supported by their U abundance mostly within the range (154–4116 ppm) in [56] granitic zircons.

The U content of kimberlite lies between 3 and 69 ppm, Y between 4 and 194 ppm, and Yb between 0.16 and 36 ppm [54]. The geochemical features in grains (MW100 and MW113) are within the range limit of kimberlitic zircons, as they are plotted within the kimberlite field in Figures 7–9. The dominant crustal origin of the western Meiganga zircons is confirmed with their U (>65 ppm) and Th (>45 ppm), Y and $\sum$REE contents, which generally fall within the range limit in [27], [54], and [65] crustal zircons. The Y (67–1867 ppm) values for the studied zircons are within the range limit in crystals from igneous rocks (e.g., 911–17,258 ppm: syenite pegmatite; 3243–20,612 ppm: nepheline-syenite pegmatite; 120–171: syenite; 83–2342 ppm: basalts; 821–4415 ppm: dolerite; 376–67,922 ppm: granitoids) [54]. Zircon saturation temperatures are a function of crystallization temperature and melt composition [75], and their relationship to Th/U ratios help to understand magmatic melt condition [60]. The calculated Ti-zircon-temperatures in Table 1, are highly heterogeneous with equal values obtained for some zircons (700 °C for MW033 and MW045), suggesting their crystallization at the same temperature. Those values compared to those for primary zircons published in [73,74], and show some correlation. The lowest values (≤697 °C) are more close to temperatures obtained for zircons from tonalites and granites, whereas higher values (700 ≥ T (°C) ≤ 787) are close to data for zircons from tonalites, rhyolitic, and dioritic rocks. Relatively high to very high values: 815 to 892 and 915 to 1065 °C, respectively, are mostly characteristics of zircons from gabbroic rocks, although the obtained temperature (815 °C for MW024) is equal to the maximum value for zircons from anorthosite found Kikkertavak Island, Nain Anorthosite Complex, Labrador studied by [73]. The Ti-zircon temperature correlations for the Western Meiganga magmatic affiliated zircons show that they are mainly composed of zircons from granitoids, anorthosite, tonalites, gabbroic and unidentified felsic intermediate rocks.

Metamorphic Affiliated Zircons

The Hf contents in the metamorphic affiliated zircons from the western Meiganga gold placer range from 9050 to 12,580 ppm, with some of the values being close to those of magmatic zircons found in this same placer. This similarity in Hf content shows that the degree of Hf substitution was almost the same in metamorphic and part of igneous zircons. The relative high Hf content (up to 12,580 ppm) shows that as for igneous zircons, they were crystallized in Hf-enriched melts. The Hf content in these zircons is greater than values that are found in zircons grown within continental rift settings [27]. They may be zircons crystallized within crustal settings during syn-tectonic to syn-metamorphic events, as their U contents are generally greater than values found in mantle-derived zircons.

The Y contents are dominantly greater than 250 ppm and are close to those found in some of the magmatic zircons from this placer, the same is valid for Nb, Ta, Sr, Ti and U contents, and Ti-in-zircon temperatures. This similarity in elemental content and temperature may be due to their similar crystallization conditions. The main difference is that the Th (2–17 ppm) and Pb (1–8 ppm) contents which are, generally, lower than quantified values in magmatic zircons, but are close or similar to some values published by [57] for zircons from Ultra-HP eclogites and metasediments. Relating the crystallization of those metamorphic zircons to Ultra-HP eclogites and metasediments is not easy as more analyses are needed. The depletion in Th and Pb contents may relate their crystallization within Th and Pb depleted melts with low degree of Th and Pb substitution. They may be re-crystallized grains, as re-crystallized zircons are often Hf-enriched and Th–Pb-depleted [65]. Other features distinguishing the metamorphic zircons from the magmatic grains is the enrichment in HREE with respect to LREE is much more variable than that observed in magmatic zircon, and the low MREE. The low MREE in metamorphic zircons is interpreted to be due to the relative depletion of these elements in their crystallization milieu [49]. Some of the zircons that possess relatively depleted HREE abundances and very small negative Eu anomalies (Eu/Eu* = 0.24–0.63), have features found in zircons grown by net transfer reactions in high-grade metamorphic rocks [57]. A negative Eu anomaly is a common feature of HT metamorphic rocks [75]. The calculated Eu anomalies and plotted data in Figure 4 for these zircons are negative and positive, with positive values found in zircon with highest Ti-zircon temperatures; contradicting the above information. Those with positive Eu anomalies were probably grown in oxidizing conditions at high temperature.

The composition of metamorphic zircon in equilibrium with an anatectic melt does not differ greatly from igneous zircons. The zircons are enriched in trace elements and have steep REE patterns increasing from La to Lu with positive Ce and negative Eu anomalies [65]. The features presented above are characteristics of MW001, and relate its crystallization in an anatectic melt. The normalized-chondrite REE data presented in Figure 4 and based on [65] studies, distinguished two main generations of zircons: those produced by sub-solidus growth in equilibrium with garnet (e.g., MW015, MW022, and MW052) and grew in equilibrium with anatectic melt (e.g., MW001). Two groups are distinguished within the first generation: (1) zircons with positive Eu anomaly and (2) grains with negative Eu anomaly. The features in group 2 zircons are common in metamorphic zircons [57], but those presented in group 1 are difficult to interpret as data on source rocks are lacking. For [76] in petrogenesis of metamorphic rocks, during high temperature metamorphism within crustal environments and at the pressure of 500 MPa, and in the presence of an aqueous fluid, granitic rocks begin to melt at a temperature of about 660 °C, whereas basaltic rocks need a much higher temperature of about 800 °C.

The measured Ti-zircon temperature in the metamorphic zircon grains ranges from 571 to 665 °C with the highest value being close to temperatures recorded at the beginning of fusion of granitic rocks. Those with relative high temperature (621 to 665 °C: close to some magmatic zircons), may be the grains crystallized at the beginning of melting of granitic parent rocks during high temperature regional metamorphism. The type of the metamorphism (subduction type or collisional type) is difficult to be determined by simple examination of geochemical features and temperature in clastic zircons, although the recorded temperature for those zircons are much closer to the highest temperatures (up to 700 °C) obtained during subduction-type orogenic metamorphism [76].

5.1.2. Detrital Zircon Geochronology and the Potential Source of Gold Placer

The recorded $^{206}Pb/^{238}U$ ages ranging from 576 ± 10 to 2927 ± 52 Ma (Table 3 and Figures 5 and 6), are highly heterogeneous, with the youngest ages (≤611 Ma) recorded mostly in metamorphic zircons and oldest ages in mainly those of a magmatic origin. Major age peaks are: Neoproterozoic, late Mesoproterozoic, late Paleoproterozoic, early Paleoproterozoic, and Archean. The metamorphic zircons were mainly crystallized during the Neoproterozoic, whereas the magmatic grains grew during Archean to early Neoproterozoic. Those suggested to crystallize by partial melt segregation were formed during Archean to Paleoproterozoic (2585 ± 45 to 1958 ± 39 Ma) with most of them being of Paleoproterozoic. The mostly magmatic nature of the zircons shows that their source areas are dominantly made of magmatic rocks and/or metamorphic rocks with inherited igneous zircons. The ages of some of the magmatic zircons are similar, suggesting that they have been crystallized at the same time and derived likely from the same rock type.

The age of the magmatic zircon grains is extremely variable, with the peak of crystallization of early Paleoproterozoic, followed by late Paleoproterozoic, late Mesoproterozoic and Archean. This shows that rocks of these ages dominantly provided part of the detritus forming the western Meiganga gold placer. A few were eroded from late Mesoproterozoic and Neoproterozoic age rocks. Within these 5 groups (Archean to early Neoproterozoic), 7 sub-groups can be distinguished with the peak being that of the Rhyacian to Orosirian (2050–1807 Ma). If they are from different source rocks, it should reflect the existence of different magmatic history in their source areas. It started during Rhyacian and continues up to Orosirian. This hypothesis is confirmed by the geochemical characteristics presented above. A single grain (MW105: Hf = 8970 ppm; age: 1922 Ma) is suggested to have crystallized within a continent rift setting, whereas the other grains (Hf > 9000 ppm) are not related to continental rifting. The same interpretation can be applied to other Paleoproterozoic zircons, which are also composed of a population crystallized within rift settings and non-rifting settings. From a general point of view, with the exception of the Mesoproterozoic and early Neoproterozoic age zircons that were exclusively not crystallized during rifting, the other zircon sub-groups are composed of those crystallized during rifting and out of rifting. What is remarkable is that the oldest zircons found in the Archean sub-group were crystallized within a continental rift setting. This shows that the magmatic history in their source of area of the Archean zircons started with rifting and mainly continued by crustal crystallization for the youngest grains, although late and post-Archean rifting were also registered.

The metamorphic zircons ranging in age from 1915 to 576 Ma ($^{206}Pb/^{238}U$ ages) are also variable; they are dominantly composed of grains crystallized during the Neoproterozoic (Ediacarian) with just one grain of Paleoproterozoic (Orosirian). The Hf (>9000 ppm) and U (>65 ppm) contents show that they grew within a crustal setting. The youngest zircons of Neoproterozoic age may be grains formed during metamorphic transformation of oldest rocks found in the source area. The heterogeneity of these ages led to the distinguishing of two generations of metamorphic events within the source area: the Orosirian (the oldest) and the Ediacarian (youngest). This also shows that rocks of those ages provided part of the sediments found in the western Meiganga gold placer. The Ediacarian grains may be zircons crystallized during Pan-African events (730–550 Ma: [77]; 850–550 Ma: [78]) fingerprinted within the Cameroon mobile zone that was formed during the Neoproterozoic, from the collision between the Saharan metacraton and the Congo Craton [29,30]. The age (1915 ± 45 Ma) of the oldest metamorphic zircon date the Eburnean tectonic and metamorphic event (2400–1800 Ma: [79]) in Cameroon.

5.2. Potential Source Rock(s) and Area(s): Implications for Siliciclastic Components

A series of ages were obtained for some rocks found within the local geological setting (e.g., in [28,35–38]). These ages are compared to those obtained in this study in order to locate the potential source rocks. The U–Pb zircon ages (2339–1887 Ma, 889–675 Ma [35]) for amphibole-biotite gneiss in Meiganga are close to the $^{206}Pb/^{238}U$ age of some of the studied detrital zircons (Table 4). The similarity is mainly for the oldest zircons; the maximum age 2339 Ma and 1887 Ma for zircons from amphibole-biotite gneiss are almost similar to 2338 Ma (MW019), 1886 Ma (MW021), and 1883 Ma (MW094) zircons. These similarities in age suggest that those zircons were probably eroded from this rock. Similarities are also observed for zircon ages of pyroxene-amphibole-bearing gneiss (≈2.6 to ≈1.6 Ga: [35,38] and meta-diorite (619 to 582 Ma: [36,38]) found in this locality (Table 4); the relationship is consistent for the pyroxene-amphibole-bearing gneiss, than metadiorite, as the youngest dated zircons from the gold placer are metamorphic, whereas zircons from meta-diorite are magmatic. Those youngest zircons were not sorted from the metadiorite, but from an unknown metamorphic rock formed during the same period. Clastic zircons whose age is close to that of pyroxene-amphibole gneiss, where likely derived from this rock. The mean zircons ages: 2645 Ma (Archean), 2309 to 1845 Ma (early to late Paleoproterozoic) obtained for two mica granite found in the western part of Meiganga [28,38], are close to the core age of some Archean (e.g., MW041: 2652 Ma) and similar to late Paleoproterozoic (e.g., MW106: 1842 Ma; MW086: 1862 Ma; MW073: 1848 Ma; MW075: 1839 Ma) zircons from the placer. This age similarity and their magmatic nature (in Figures 7–9) indicate that part the oldest zircons were sorted from the two mica-rich granitic rock.

Table 4. Possible correlations between the ($^{206}Pb/^{238}U$) age of the western Meiganga detrital zircons and that of zircon from rocks published in [37,44–47].

PAGn Age (Ma)	NWD-Zircon Age (Ma)	ABGn Age (Ma)	MWD-Zircon Age (Ma)	ABGn Age (Ma)	MWD-Zircon Age (Ma)	M-D Age (Ma)	NWD-Zircon Age (Ma)
1813.7 ± 3.4		1887.6 ± 2.1	1886 ± 30	768.7 ± 4.1		614.3 ± 5.8	611 ± 12
1711.7 ± 3.4		1955.6 ± 2.6	1958 ± 39	877.5 ± 3.3		622.3 ± 3.0	
1685.0 ± 4.0	1643 ± 31	1963.8 ± 2.5		879.6 ± 2.9		626.6 ± 4.6	
2453.4± 4.3		1983.7 ± 1.7		721.3 ± 3.3		582.1 ± 7.8	
2512.3 ± 3.4		1988.0 ± 1.9	1986 ± 38	811.9 ± 3.0		584.2 ± 7.6	584 ± 11
2478.2± 3.3	2463 ± 50	2005.5± 1.8	2007 ± 35	845.0 ± 3.4		619.0 ± 5.4	
2430.7± 3.4		2022.8 ± 2.1		740.4 ± 6.5		633.2 ± 3.9	
2504.3± 3.7	2500 ± 70	2099.3 ± 0.9		859.2 ± 4.0		620.7 ± 4.8	
2602.6 ± 13.5		2153.7± 1.4		887.1 ± 6.6		627.1 ± 8.1	
2170.0± 4.0	2171 ± 36	2269.0± 2.5		753.5 ± 4.3			
2274.5 ± 3.3	2269 ± 60	2319.7± 1.7		814.4 ± 6.2			
2387.8 ± 4.6		2339.4 ± 2.6	2338 ± 44	889.4 ± 2.3			
2398.2± 4.1				675.1 ± 7.0			
2514.0 ± 3.5				829.1 ± 6.2	834 ± 18		
2578.2 ± 4.0	2583 ± 55						

PAGn: Pyroxene-amphibole gneiss; MWD-Zircon: Western Meiganga detrital zircon, ABGn: Amphibole-biotite gneiss; M-D: Meta-diorite.

It is possible to establish some correlations within the regional geological settings based on their provenance, paleoweathering and paleotectonic conditions [80]. The Archean ages for the western Meiganga detrital zircons are close to the ages of TTG and other rocks found in Congo Craton (Table 5). The ages (early to late Archean) of the oldest grains are similar to those of some charnockites, tonalites, granodiorites and high-K-granites, found in the Ntem Complex in the north western part of the Congo Craton. This age similarities show the studied zircons and those found in rocks presented above were probably crystallized during the same period (early to late Archean). The Mesoproterozoic and part of Paleoproterozoic grains also have the same age range as those found in, Yobé granite (Cameroon), Doum-Lolodorf and Mengueme syenites, meta dolerite dykes, charnockites, and granodiorites in Sangmelima (Table 5). This similarity in age shows that these zircons and those found in the above rocks were crystallized during the same period.

Table 5. Possible correlations between the ($^{206}Pb/^{238}U$) age of the western Meiganga detrital zircons and that of zircons from some rocks within regional geological settings.

Locality and Author (s)	Method	Rock Type	Age (Ma)	Age of MWD-Zircon (Ma)
Sangmelima [68]	Rb–Sr biotite dating	Granodiorite	1997 ± 19	1996 ± 39,1993 ± 36, 1992 ± 38
		Charnockite	2064 ± 20, 2299 ± 22	2059 ± 40, 2255 ± 43, 2269 ± 60
Sangmelima [62]	Pb-evaporation zircon dating	Charnockites	2792 ± 4 2689 ± 20 2671 ± 25	2789 ± 51 2680 ± 84 2637 ± 47
		Granodiorites	2686 ± 31 2674 ± 21 2920 ± 7 2933 ± 13 2939 ± 13 2962 ± 11	2627 ± 45 2927 ± 52 2913 ± 51 2907 ± 65
		Tonalites	2678 ± 17	2680 ± 84
Sangmelima [69]	Pb-evaporation zircon dating	High-K granites	2175 ± 11 2218.4 ± 4.0 2302.3 ± 1.7 2345.5 ± 5.1 2386 ± 2.7 2403.2 ± 8.2 2424.4 ± 2.9 2427.9 ± 8.7 2428.2 ± 3.1 2435.4 ± 5.2 2481.6 ± 3.2 2487.4 ± 3.7 2496.1 ± 2.3 2506.5 ± 4.2 2509 ± 3.2 2512.0 ± 7.9 2565.8 ± 7.4 2565 ± 19 2591.6 ± 4.3 2598.3 ± 8.0 2600.9 ± 3.2 2614.5 ± 4.9 2622 ± 14 2631.9 ± 3.9 2657.7 ± 2.7 2682.6 ± 1.8 2684.6 ± 6.8 2688.8 ± 2.7 2719.4 ± 3.4 2721.2 ± 1.5 2720.6 ± 3.2 2788 ± 35	2122 ± 36 2125 ± 52 2171 ± 36 2173 ± 40 2200 ± 69 2210 ± 39 2190 ± 51 2255 ± 43 2338 ± 40 2363 ± 40 2401 ± 43 2407 ± 43 2425 ± 46 2433 ± 44 2458 ± 46 2463 ± 50 2485 ± 46 2487 ± 50 2500 ± 70 2530 ± 48 2564 ± 44 2570 ± 57 2590 ± 54 2583 ± 55 2585 ± 45 2680 ± 84 2637 ± 47 2627 ± 45 2789 ± 51

Table 5. *Cont.*

Locality and Author (s)	Method	Rock Type	Age (Ma)	Age of MWD-Zircon (Ma)
Ebolawa [81]	U–Pb zircon dating Rb/Sr isochrons	Charnockites	2896 ± 7 2882 ± 70	2913 ± 51, 2907 ± 65
Northern border of the Congo Craton [82]	Pb-evaporation zircon dating	Charnockites	2912 ± 25	2907 ± 65
		Tonalite	2833 ± 15	
South Region of Cameroon [79]	Rb/Sr isochrons	Granodiorites	2880 ± 70	2913 ± 51, 2907 ± 65
South Region of Cameroon [81,83]	Sm–Nd whole rocks isochron	Meta-doleritedikes	2059 ± 16	2059 ± 40, 2053 ± 38
Doum–Lolodorf and Mengueme [84]	Pb-evaporation zircon dating	Two pyroxene syenite	2321 ± 1	2269 ± 60
		Clinopyroxene syenite	2349 ± 1, 2667 ± 1	2637 ± 47
Yobé –Cameroon [85]	Rb/Sr isochrons	Granites	1167 ± 61	1162 ± 21, 1096 ± 24

The source rocks of those detrital zircons are the same nature as those described above (syenitic, doleritic, charnockitic, or granitic) that are distinguished from their geochemical variations. The Neoproterozoic ages (611–576 Ma) of the youngest zircons found within the western Meiganga placer overlap the range of ages for Pan-African zircons found along the Cameroon mobile belt, indicating their crystallization period and has implications on tracking gold placer source(s).

6. Conclusions

The western Meiganga detrital zircons are highly heterogeneous detritus crystallized in chemically enriched and depleted magmatic and metamorphic rocks. The magmatic zircons were crystallized and probably eroded from granitoids, syenites, kimberlites, tonalites, charnockites, and/or unidentified mafic rocks. Their ages of crystallization are Archean, early and late Paleoproterozoic, late Mesoproterozic, and Neoproterozoic. The Neo-archean zircons are inherited crystals and were probably eroded from local pyroxene-amphibole gneiss. Part of the late Paleoproterozoic zircons were probably sorted from two mica granite found in the west of Meiganga. The source of early Proterozoic zircons can possibly be the amphibole-biotite gneiss. The sources of the other grains, with ages close to those of some magmatic rocks are found within the Congo Craton in the South of Cameroon remain to be determined locally.

The metamorphic zircons (late Paleoproterozoic and Neoproterozoic in age) were formed during two tectono-metamorphic events: the Eburnean and Pan- African.

Author Contributions: Kanouo Sylvestre Nguo, Ngueutchoua Gabriel and Kouske Patrice Arnaud, presented and interpreted the results, and conceived the research paper. Yongue Fouateu Rose and Venkatesh Satya Akella edited the paper and also contributed to revise the paper at different stages of the reviewing process.

Acknowledgments: The authors are grateful to personnel of Department Earth Sciences and Earth Research Institute, University of California, Santa Barbara, CA, USA, for the financial support and laboratory facilities during the geochemical analyses and U–Pb dating of the western Meiganga detrital zircons. Special thanks to John Cottle of the University of California for financing and analyzing the zircons and for his valuable suggestions. The authors extend their gratitude and thanks to David Richard Lentz at the University of New Brunswick for his insightful comments and initial reviews on this manuscript. The authors thank Editor, Associate Editor and reviewers for their useful comments.

Conflicts of Interest: The authors declare no conflict of interest.

References

1. Evans, M.A. *Ore Geology and Industrial Minerals: An Introduction*, 3rd ed.; Backwell Pubishing: Hoboken, NJ, USA, 1993; p. 403.
2. Force, E.R. Placer Deposits. In *Sedimentary and Diagenetic Mineral Deposits, a Basin Analysis Approach to Exploration*; Force, E.R., Eidel, J.J., Maynard, J.B., Eds.; Economic Geologic Society: Littleton, CO, USA, 1991.

3. Robb, L. *Introduction to Ore-Forming Processes*; Backwell Publishing: Hoboken, NJ, USA, 2005; p. 386.
4. Eynatten, V.H.; Gaupp, R. Provenance of Cretaceous synorogenic sandstones in the Eastern Alps: Constraints from framework petrography, heavy mineral analysis and mineral chemistry. *J. Sed. Geol.* **1999**, *124*, 81–111. [CrossRef]
5. Morton, C.A.; Claoue-Long, C.J.; Hallsworth, C.R. Zircon age and heavy mineral constraints of North Sea Carboniferous sandstones. *Mar. Pet. Geol.* **2001**, *18*, 319–337. [CrossRef]
6. Pakhomova, A.V.; Zalishchak, L.B.; Odarichenko, G.E.; Lapina, I.M.; Karmanov, S.N. Study of melt inclusions in the Nezametnoye corundum deposit, Primorsky region of the Russian Far East: Petrogenetic consequences. *J. Geochem. Explor.* **2006**, *89*, 302–305. [CrossRef]
7. Zack, T.; Eynatten, V.H.; Kronz, A. Rutile geochemistry and its potential use in quantitative provenance studies. *J. Sed. Geol.* **2004**, *171*, 37–58. [CrossRef]
8. McClenaghan, B.M. Overview of processing methods for recovery of indicator minerals from sediment and bedrock samples. In Proceedings of the Workshop in the 25th International Applied Geochemistry Symposium, Rovaniemi, Finland, 22–26 August 2011; p. 72.
9. Kanouo, S.N.; Yongue, F.R.; Shouyu, C.; Njonfang, E.; Ma, C.; Ghogumo, T.R.; Jiangnan, Z.; Sababa, E. Greyish black rutile megaclasts from the Nsanaragati Gem Placer, SW Cameroon: Geochemical features and genesis. *J. Geogr. Geol.* **2012**, *3*, 134–146. [CrossRef]
10. Kanouo, S.N.; Zaw, K.; Yongue, F.R.; Sutherland, L.F.; Meffre, S.; Njonfang, E.; Ma, C.; Tchouatcha, S.T. U–Pb zircon age constraining the source and provenance of gem-bearing Late Cenozoic detrital deposit, Mamfe Basin, SW Cameroon. *Resour. Geol.* **2012**, *62*, 316–324. [CrossRef]
11. Kanouo, S.N.; Yongue, F.R.; Ekomane, E.; Njonfang, E.; Ma, C.; Lentz, D.R.; She, Z.; Zaw, K.; Venkatesh, A.S. U–Pb ages for zircon grains from Nsanaragati Alluvial Gem Placers: Its correlation to the source rocks. *Resour. Geol.* **2015**, *65*, 103–121. [CrossRef]
12. Kanouo, S.N.; Ekomane, E.; Yongue, F.R.; Njonfang, E.; Zaw, K.; Ma, C.; Ghogomu, R.T.; Lentz, D.R.; Venkatesh, A.S. Trace elements in corundum, chrysoberyl, and zircon: Application to mineral exploration and provenance study of the western Mamfe gem clastic deposits (SW Cameroon, Central Africa). *J. Afr. Earth Sci.* **2016**, *113*, 35–50. [CrossRef]
13. Kanouo, S.N. Geology of the Western Mamfe Corundum Deposits, SW Region Cameroon: Petrography, Geochemistry, Geochronology, Genesis, and Origin. Ph.D. Thesis, University of Yaoundé I, Yaoundé, Cameroon, 2014.
14. Taivalkoski, A.; Sarala, P.; Hulkki, H. Gold exploration using heavy minerals in till and weathered bedrock in Petäjäselkä, northern Finland. *Geochem. Explor. Env. Analy.* **2013**, *15*, 205–221. [CrossRef]
15. Mbih, P.K.; Meffre, S.; Yongue, F.R.; Kanouo, S.N.; Thomson, J. Chemistry and origin of the Mayo Kila sapphires, NW region Cameroon (Central Africa): Their possible relationship with the Cameroon volcanic line. *J. Afr. Earth Sci.* **2016**, *118*, 263–273. [CrossRef]
16. Fedo, M.C.; Keith, N.S.; Robert, H.R. Detrital Zircon Analysis of the Sedimentary Record. In *Reviews in Mineralogy and Geochemistry*; Mineralogical Society of America: Washington, DC, USA, 2003; Volume 53, pp. 277–333.
17. Murphy, B.J.; Fernandez-Suarez, J.; Jeffries, T.; Strachan, R. U–Pb (LA-ICP-MS) dating of detrital zircons from Cambrian clastic rocks in Avalonia: Erosion of a Neoproterozoic arc along the northern Gondwana margin. *J. Geol. Soc. Lond.* **2004**, *161*, 243–254. [CrossRef]
18. Paulsen, T.; Deering, C.; Sliwinski, J.; Bachmann, O.; Guillong, M. New detrital zircon age and trace element evidence for 1450 Ma igneous zircon sources in East Antarctica. *Precambrian Res.* **2017**, *300*, 53–58. [CrossRef]
19. Veevers, J.J.; Belousova, A.E.; Saeed, A.; Sircombe, K.; Cooper, F.A.; Read, E.S. Pan-Gondwanaland detrital zircons from Australia analyzed for Hf-isotopes and trace elements reflect an ice-covered Antarctic provenance of 700–500 Ma age, TDM of 2.0–1.0 Ga, and alkaline affinity. *Earth Sci. Rev.* **2006**, *76*, 135–174. [CrossRef]
20. Belousova, E.A.; Kostitsyn, Y.A.; Griffin, W.L.; Begg, G.C.; O'Reilly, S.Y.; Pearson, N.J. The growth of the continental crust: Constraints from zircon Hf-isotope data. *Lithos* **2010**, *119*, 457–466. [CrossRef]
21. Dickinson, W.R.; Gehrels, G.E. Use of U–Pb ages of detrital zircons to infer maximum depositional ages of strata: A test against a Colorado Plateau Mesozoic database. *Earth. Planet. Sci. Lett.* **2009**, *288*, 115–125. [CrossRef]

22. Makoundi, C.; Zaw, K.; Large, R.R.; Meffre, S.; Chun-Kit, L.; Hoe, G.T. Geology, geochemistry and metallogenesis of the Selinsing gold deposit, central Malaysia. *Gondwana Res.* **2013**, *26*, 241–261. [CrossRef]
23. McQuarrie, N.; Long, P.S.; Tobgay, T.; Nesbit, N.J.; Gehrels, G.; Ducea, N.M. Documenting basin scale, geometry and provenance through detrital geochemical data: Lessons from the Neoproterozoic to Ordovician Lesser, Greater, and Tethyan Himalayan strata of Bhutan. *Gondwana Res.* **2013**, *23*, 1491–1510. [CrossRef]
24. Kanouo, S.N.; Njonfang, E.; Kouské, P.A.; Yongue, F.R.; Ngueutchoua, G. U–Pb zircon age: Preliminary data evaluating the Earth history recorded by two basement rocks (granitic pegmatite and mica-Schist) in Mamfe Basin (SW Cameroon, Central Africa). *J. Geol. Geophys.* **2017**, *6*, 1–9. [CrossRef]
25. Kresten, P.; Fels, P.; Berggren, G. Kimberlite zircons a possible aid in prospecting for kimberlites. *Miner. Depos.* **1975**, *10*, 47–56. [CrossRef]
26. Sutherland, L.F.; Meffre, S. Zircon megacryst age and chemistry, from a placer, Dunedin volcanic area, eastern Otago, New Zealand. *N. Z. J. Geol. Geophys.* **2009**, *52*, 185–194. [CrossRef]
27. Heaman, L.M.; Bowins, R.; Crocket, J. The chemical composition of igneous zircon suites: Implications for geochemical tracer studies. *Geochem. Cosmochem. Acta* **1990**, *54*, 1597–1607. [CrossRef]
28. Ganwa, A.A. Les Granitoïdes de Méiganga: Etude Pétrographique, Géochimique, Structurale et Géochronologique. Leur Place Dans la Chaîne Panafricaine. Thèse de Doctorat d'État ès Sciences Naturelles, Université de Yaoundé I, Yaoundé, Cameroon, 2005.
29. Abbelsalam, G.M.; Liégeois, P.J.; Stern, J.R. The Saharan Metacraton. *J. Afr. Earth Sci.* **2002**, *34*, 119–136. [CrossRef]
30. Ngako, V.; Njonfang, E.; Affaton, P. Pan-African tectonics in northwestern Cameroon: Implication for the history of the western Gondwana. *Gondwana Res.* **2008**, *14*, 509–522. [CrossRef]
31. Nzenti, J.P.; Barbey, P.; Macaudiere, J.; Soba, D. Origin and evolution of the Late Precambrian high-grade Yaoundé gneisses (Cameroon). *Precambrian Res.* **1988**, *38*, 91–109. [CrossRef]
32. Nzenti, J.P. Neoproterozoic alkaline meta-igneous rocks from the Pan-African north Equatorial Fold Belt (Yaoundé, Cameroon): Biotitites and magnetite rich pyroxenites. *J. Afr. Earth Sci.* **1998**, *26*, 37–47. [CrossRef]
33. Toteu, F.S.; Van Schmus, W.R.; Penaye, J.; Michard, A. New U–Pb and Sm–Nd data from north-central Cameroon and it bearing on the Pre-Pan African history of Central African. *Precambrian Res.* **2001**, *108*, 45–73. [CrossRef]
34. Ngako, V.; Affaton, P.; Nnangue, J.M.; Njanko, T. Pan-African tectonic evolution in central and southern Cameroon: Transpression and transtension during sinistral shear movements. *J Afr. Earth Sci.* **2003**, *36*, 207–214. [CrossRef]
35. Ganwa, A.A.; Frisch, W.; Siebel, W.; Ekodeck, E.G.; Shang, K.C.; Ngako, V. Archean Inheritances in the Pyroxene-Amphibole-Bearing Gneiss of the Méiganga Area (Central North Cameroon): Geochemical and $^{207}Pb/^{206}Pb$ Age Imprints. *C. R. Geosci.* **2008**, *340*, 211–222. [CrossRef]
36. Ganwa, A.A.; Siebel, W.; Shang, K.C.; Naimou, S.; Ekodeck, G.E. New Constraints from Pb-Evaporation Zircon Ages of the Méiganga Amphibole-Biotite Gneiss, Central Cameroon, on Proterozoic Crustal Evolution. *Int. J. Geosci.* **2011**, *2*, 138–147.
37. Ganwa, A.A.; Frisch, W.; Siebel, W.; Shang, C.K. Geochemistry of Magmatic Rocks and Time Constraints on Deformational Phases and Shear Zone Slip in the Méiganga Area, Central Cameroon. *Int. Geol. Rev.* **2011**, *53*, 759–784. [CrossRef]
38. Ganwa, A.A.; Klotzli, S.U.; Hauzenberger, C. Evidence for Archean inheritance in the pre-Panafrican crust of Central Cameroon: Insight from zircon internal structure and LA-MC-ICP-MS U–Pb ages. *J. Afr. Earth Sci.* **2016**, *120*, 12–22. [CrossRef]
39. Tetsopgang, S.; Suzuki, K.; Njonfang, E. Petrology and CHIME geochronology of Pan-African high K and Sr/Y granitoids in the Nkambe area, Cameroon. *Gondwana Res.* **2008**, *14*, 686–699. [CrossRef]
40. Lasserre, M. *Etude Géologique de la Partie Orientale de L'adamaoua (Cameroun Central) et les Principales Sources Minéralisées de L'adamaoua*; Université de Clermont-Ferrand: Clermont-Ferrand, France, 1961.
41. Kenna, H.S. Prospection des Indices de Minéralisations d'or Dans la Zone de Meiganga Ouest. Master's Thesis, Université de Yaoundé I, Yaoundé, Cameroon, 2015.
42. Moles, N.; Chapman, R. Placer gold microchemistry in conjunction with mineralogy and mineral chemistry of heavy mineral concentrates to characterize bedrock sources. In Proceedings of the 25th International Applied Geochemistry Symposium, Rovaniemi, Finland, 22–26 August 2011; pp. 19–25.

43. Parfenoff, A.; Pomerol, C.; Tourenq, J. *Les Minéraux en Grains. Méthodes D'étude et Détermination*; Masson et Cie Edition: Paris, France, 1970; p. 571.
44. Mange, A.M.; Maurer, W.F.H. *Heavy Minerals in Colour*, 1st ed.; Chapman and Hall: London, UK, 1992; p. 154.
45. Cottle, J.M.; Waters, D.J.; Riley, D. Metamorphic history of the South Tibetan Detachment System, Mt. Everest region, revealed by RSCM thermometry and phase equilibria modelling. *J. Metamorph. Geol.* **2011**, *29*, 561–582. [CrossRef]
46. Cottle, J.M.; Burrows, A.J.; Kylander-Clark, A.; Freedman, P.A.; Cohen, R. Enhanced sensitivity in laser ablation multi-collector inductively coupled plasma mass spectrometry. *J. Anal. At. Spectrom.* **2013**. [CrossRef]
47. Kylander-Clark, A.R.C.; Hacker, B.R.; Cottle, J.M. Laser-ablation split-stream ICP petrochronology. *Chem. Geol.* **2013**, *345*, 99–112. [CrossRef]
48. Paton, C.; Woodhead, J.; Hellstrom, J.; Hergt, J.; Greig, A.; Maas, R. Improved laser ablation U–Pb zircon geochronology through robust down hole fractionation correction. *Geochem. Geophys. Geosyst.* **2010**, *11*. [CrossRef]
49. Wiedenbeck, M.; Alle, P.; Corfu, F.; Grin, W.; Meier, M.; Oberli, F.; Von Quadt, A.; Roddick, J.; Spiegel, W. Three natural zircon standards for U–Th–Pb, Lu–Hf, trace element and REE analyses. *Geostand. Newslett.* **1995**, *19*, 1–23. [CrossRef]
50. Jackson, S.; Pearson, N.; Griffin, W.; Belousova, E. The application of laser ablation-inductively coupled plasma-mass spectrometry to in situ U/Pb zircon geochronology. *Chem. Geol.* **2004**, *657*, 47–69. [CrossRef]
51. Ludwig, K. *User's Manual for Isoplot 2.4: A Geochronological Toolkit for Microsoft Excel*; Berkeley Geochronology Center: Berkeley, CA, USA, 2012.
52. Vermeesch, P. On the visualisation of detrital age distributions. *Chem. Geol.* **2012**, *312–313*, 190–194. [CrossRef]
53. Steiger, R.; Jager, E. Subcommission on geochronology: Convention on the use of decay constants in geo- and cosmochronology. *Earth Planet. Sci. Lett.* **1977**, *36*, 359–362. [CrossRef]
54. Belousova, A.E.; Griffin, L.W.; O'Reilly, Y.S.; Fisher, I.N. Igneous zircon: Trace element composition as an indicator of source rock type. *J. Miner. Petrol.* **2002**, *143*, 602–622. [CrossRef]
55. Dawaï, D.; Jean-Luc Bouchez, L.J.; Paquette, L.J.; Tchameni, R. The Pan-African quartz-syenite of Guider (north-Cameroon): Magnetic fabric and U–Pb dating of a late orogenic emplacement. *Precambrian Res.* **2013**, *236*, 132–144. [CrossRef]
56. Ahrens, L.H.; Cherry, R.D.; Erlank, A.J. Observations on the Th–U relationship in zircons from granitic rocks and from kimberlites. *Geochim Cosmochim. Acta* **1967**, *31*, 2379–2387. [CrossRef]
57. Rubatto, D. Zircon trace element geochemistry: Partitioning with garnet and link between U–Pb ages and metamorphism. *Chem. Geol.* **2002**, *184*, 123–138. [CrossRef]
58. Konzett, J.; Armstrong, R.A.; Sweeny, R.J.; Compston, W. The timing of Marid suite metasomatism in the Kaapvaal mantle: An ion probe study of zircons from Marid xenoliths. *Earth Planet. Sci. Lett.* **1998**, *160*, 133–145. [CrossRef]
59. McDonough, F.W.; Sun, S.S. The composition of the Earth. *Chem. Geol.* **1995**, *120*, 223–253. [CrossRef]
60. Kirkland, C.L.; Smithies, R.H.; Taylor, R.J.M.; Evans, N.; McDonald, B. Zircon Th/U ratios in magmatic environs. *Lithos* **2015**, *212–215*, 397–414. [CrossRef]
61. Sutherland, F.L.; Coenraads, R.R.; Abduryim, A.; Meffre, S.; Hoskin, O.W.P.; Giuliani, G.; Beattie, R.; Wuhrer, R.; Sutherland, B.G. Corundum (sapphire) and zircon relationships, Lava Plains gem fields, NE Australia: Integrated mineralogy, geochemistry, age determination, genesis and geographical typing. *Miner. Mag.* **2015**, *79*, 545–581. [CrossRef]
62. Shang, C.K.; Satir, M.; Siebel, W.; Nsifa, E.N.; Taubald, H.; Liegeois, J.P.; Tchoua, F.M. Major and trace element geochemistry, Rb–Sr and Sm–Nd systematics of TTG magmatism in the Congo craton: Case of the Sangmelima region, Ntem complex, southern Cameroon. *J. Afr. Earth Sci.* **2004**, *40*, 61–79. [CrossRef]
63. Wan, Y.; Liu, D.; Dong, C.; Liu, S.; Wang, S.; Yang, E. U–Th–Pb behavior of zircons under high-grade metamorphic conditions: A case study of zircon dating of met-adiorite near Qixia, eastern Shandong. *Geosci. Front.* **2011**, *2*, 137–146. [CrossRef]
64. Hiess, J.; Nutman, A.P.; Bennett, V.C.; Holden, P. Ti-in-zircon thermometry applied to contrasting Archean metamorphic and igneous systems. *Chem. Geol.* **2008**, *247*, 323–338. [CrossRef]
65. Hoskin, P.W.O.; Schaltegger, U. The composition of zircon and igneous and metamorphic petrogenesis. In *Reviews in Mineralogy and Geochemistry*; Mineralogical Society of America: Washington, DC, USA, 2003; Volume 53, pp. 27–55.

66. Kröner, A.; Jaeckel, P.; Williams, I.S. Pb-loss patterns in zircons from a high grade metamorphic terrain as revealed by different dating methods: U–Pb and Pb–Pb ages of igneous and metamorphic zircons from Northern Sri Lanka. *Precambrian Res.* **1994**, *66*, 151–181. [CrossRef]
67. Whitehouse, M.J.; Kamber, B.S.; Moorbath, S. Age significance of U–Th–Pb zircon data from early Archean rocks of west Greenland-a reassessment based on combined ion-probe and imaging studies. *Chem. Geol.* **1999**, *160*, 201–224. [CrossRef]
68. Shang, C.K.; Siebel, W.; Satir, M.; Chen, F.; Mvondo, J.O. Zircon Pb–Pb and U–Pb systematics of TTG rocks in the Congo craton: Constraints of crustal formation, crystallization and Pan-African lead loss. *Bull. Geosci.* **2004**, *79*, 205–219.
69. Shang, K.C.; Liégeois, P.J.; Satir, M.; Frisch, W.; Nsifa, E.N. Late Archaean high-K granite geochronology of the northern metacratonic margin of the Archaean Congo craton, Southern Cameroon: Evidence for Pb-loss due to non-metamorphic causes. *Gondwana Res.* **2010**. [CrossRef]
70. Watson, E.B.; Wark, A.D.; Thomas, B.J. Crystallization thermometers for zircon and rutile. *Contrib. Miner. Petrol.* **2006**, *151*, 413–433. [CrossRef]
71. Cherniak, D.J.; Watson, E.B. Ti diffusion in zircon. *Chem. Geol.* **2007**, *242*, 470–483. [CrossRef]
72. Murali, A.V.; Parthasarathly, R.; Mahadevan, T.M.; Sankar Das, M. Trace elements characteristics, REE patterns and partition coefficient of zircons from different geological environment-A case study of Indian zircons. *Geochem. Cosmochem. Acta* **1983**, *47*, 2047–2052. [CrossRef]
73. Fu, B.; Page, F.Z.; Cavosie, A.J.; Fournelle, J.; Kita, N.T.; Lackey, J.S.; Wilde, S.A.; Valley, J.W. Ti-in-zircon thermometry: Applications and limitations. *Contrib. Miner. Petrol.* **2008**. [CrossRef]
74. Grimes, C.B.; John, E.B.; Cheadle, J.M.; Mazdab, K.F.; Wooden, L.J.; Swapp, S.; Schwartz, J.J. On the occurrence, trace element geochemistry, and crystallization history of zircon from in situ ocean lithosphere. Contrib. *Miner. Petrol.* **2009**. [CrossRef]
75. Hoskin, P.W.O.; Black, L.P. Metamorphic zircon formation by solid-state recrystallization of protolith ignous zircon. *J. Met. Petrol.* **2000**, *18*, 423–439. [CrossRef]
76. Bucher, K.; Grapes, R. *Petrogenesis of Metamorphic Rocks*, 8th ed.; Springer: Berlin/Heidelberg, Germany, 2011; p. 441.
77. Black, R.; Liegeois, P.J. Cratons, mobile belts, alkaline rocks and continental lithospheric mantle: The Pan-African testimony. *J. Geol. Soc. Lond.* **1993**, *150*, 89–98. [CrossRef]
78. Kröner, A.; Stern, J.R. *Pan-African Orogeny*; Encyclopedia of Geology; Elsevier: Amsterdam, The Netherlands, 2004; Volume 1, pp. 1–12.
79. Lasserre, M.; Soba, D. Age Libérien des granodiorites et des gneiss à pyroxènes du Cameroun Méridional. *Bull. BRGM* **1976**, *2*, 17–32.
80. Kumar, A.; Venkatesh, A.S.; Kumar, P.; Rai, A.K.; Parihar, P.S. Geochemistry of Archean Radioactive Quartz Pebble Conglomerates and Quartzites from western margin of Singhbhum-Orissa Craton, eastern India: Implications on Paleo-weathering, Provenance and Tectonic Setting. *Ore Geol. Rev.* **2017**, *89*, 390–406. [CrossRef]
81. Toteu, S.F.; Van Schmus, W.R.; Penaye, J.; Nyobé, J.B. U–Pb and Sm–Nd evidence for Eburnean and Pan-African high-grade metamorphism in cratonic rocks of southern Cameroon. *Precambrian Res.* **1994**, *108*, 45–73. [CrossRef]
82. Pouclet, A.; Tchameni, R.; Mezger, K.; Vidal, M.; Nsifa, E.; Shang, C.; Penaye, J. Archean crustal accretion at the northern border of the Congo Craton (South Cameroon). The charnockite-TTG link. *Bull. Soc.* **2007**, *5*, 331–342.
83. Vicat, J.P.; Leger, J.M.; Nsifa, E.; Piguet, P.; Nzenti, J.P.; Tchameni, R.; Pouclet, A. Distinction au sein du craton congolais du Sud-Ouest du Cameroun, de deux episodes doleritiques initiant les cycles orogeniques eburneen (Paleoproterozoïque) et Pan-Africain (Neoproterozoïque). *C. R. Acad. Sci.* **1996**, *323*, 575–582.
84. Tchameni, R.; Mezger, K.; Nsifa, N.E.; Pouclet, A. Crustal origin of Early Proterozoic syenites in the Congo craton (Ntem complex), South Cameroon. *Lithos* **2001**, *57*, 23–42. [CrossRef]
85. Vicat, J.P.; Pouclet, A.; Nkoumbou, C.; Mouangué, S.A. The fissural volanisms of Lower Dja, Yokadouma (Cameroon) and Nola (RCA) Series-Geotectonic meaning. *C. R. Acad. Sci.* **1997**, *325*, 671–677.